Technische Universität München

SLR long-term mean range biases for LEO satellites

Kristina Heinze

Master's Thesis

Study Course:	Geodesy and Geoinformation (Master)
Supervisors:	Dr.-Ing. Mathis Bloßfeld Deutsches Geodätisches Forschungsinstitut (DGFI-TUM) Technical University of Munich Prof. Dr.-Ing. habil. Florian Seitz Deutsches Geodätisches Forschungsinstitut (DGFI-TUM) Technical University of Munich
Submission	30th March 2022

2022

Declaration

With this statement I declare that I have independently completed this Master's thesis. The thoughts taken directly or indirectly from external sources are properly marked as such. This thesis was not previously submitted to another academic institution and has also not yet been published.

Munich, 30th March 2022

Kristina Heinze

Abstract

Satellite Laser Ranging (SLR) is responsible for determining the origin of the International Terrestrial Reference Frame (ITRF). Together with Very Long Baseline Interferometry (VLBI), SLR defines the scale of the ITRF. To provide accurate results, the time measurements between the station and the satellite must be free of systematic errors (range bias, RB). So far, mean RBs are determined only for the four satellites LAGEOS-1/2 and Etalon-1/2. In this thesis, the first computation of mean RBs for the seven Low Earth Orbit (LEO) satellites Ajisai, Starlette, Stella, WESTPAC 1, Larets, LARES, and BLITS is performed to clarify whether an 11-satellite solution can be used for the ITRF with the same validity of a 4-satellite solution. Based on weekly RBs data, long-term mean RBs are calculated for the respective stations. For this purpose, a method is developed to gradually summarize the periods of low fluctuating RB values. Outliers are detected in advance and removed from the data set. Two options are determined regarding the station selection, for which mean RBs are to be calculated. The selection criteria are the number of RBs and the number of RBs per year, respectively. To validate the method, the defined time periods and the corresponding mean RBs are compared to the values from the Data Handling File (DHF) of the International Laser Ranging Service (ILRS). It is shown that the results are comparable. Further, orbits are calculated for all satellites of the 4- and the 11-satellite solution. The orbits of the weekly solutions and the orbits of the DTRF2020 solution (TRF of the Deutsches Geodätisches Forschungsinstitut (DGFI-TUM)) are used for validation. The orbits of the 4-satellite solution are similar to the orbits of the DTRF2020 solution. With the newly determined RBs, the orbit parameters of LAGEOS-1 can be improved. The orbit parameters of option 2 are closer to the reference values than the orbits of option 1. Subsequent calculation and consideration of the datum parameters shows that the annual amplitude of the 11-satellite solution is higher than that of the 4-satellite solution. The mean scale of the 11-satellite solution is 2 mm higher than that of the 4-satellite solution.

Zusammenfassung

Satelliten-Laserentfernungsmessungen (SLR) sind für die Bestimmung des Ursprungs des Internationalen Terrestrischen Referenzrahmens (ITRF) zuständig. Gemeinsam mit Radiointerferometrie (VLBI) legt SLR den Maßstab des ITRFs fest. Um genaue Ergebnisse liefern zu können, müssen die Zeitmessungen zwischen der Station und dem Satelliten frei von systematischen Fehlern (Range bias, RB) sein. Bisher werden nur für die vier Satelliten LAGEOS-1/2 und Etalon-1/2 mittlere RBs bestimmt. Im Rahmen dieser Arbeit erfolgt die erstmalige Berechnung der mittleren RBs für die sieben LEO Satelliten Ajisai, Starlette, Stella, WESTPAC 1, Larets, LARES und BLITS, um abzuklären ob eine 11-Satelliten Lösung mit gleicher Aussagekraft wie eine 4-Satelliten Lösung für den ITRF genutzt werden kann. Ausgehend von wöchentlichen RB Daten, werden mittlere RBs über möglichst lange Beobachtungszeiträume für die jeweiligen Stationen berechnet. Hierfür wird eine Methode entwickelt mit der schrittweise die Zeiträume gering schwankender RB Werte zusammengefasst werden. Ausreißer werden vorab detektiert und aus der Datenreihe entfernt. Hinsichtlich der Stationsauswahl, für welche mittlere RBs berechnet werden sollen, werden zwei Optionen bestimmt. Die Auswahlkriterien sind die Anzahl der RBs bzw. die Anzahl der RBs pro Jahr. Zur Validierung der Methode werden die gefundenen Zeitabschnitte und die dazugehörigen Mittelwerte mit den Werten aus dem Data Handling File (DHF) des Internationalen Laser Ranging Services (ILRS) verglichen. Dabei zeigt sich, dass die Ergebnisse vergleichbar sind. Weiter werden Orbits für alle Satelliten der 4- und der 11-Satelliten Lösung berechnet. Zur Validierung werden die Orbits der wöchentlichen Lösungen und die Orbits der DTRF2020 Lösung (TRF des Deutschen Geodätischen Forschungsinstituts (DGFI-TUM)) verwendet. Die Orbits der 4-Satelliten Lösung sind ähnlich zu den Orbits der DTRF2020 Lösung. Mit den neu bestimmten RBs können die Orbit Parameter von LAGEOS-1 verbessert werden. Die Orbit Parameter der Option 2 zeigen größere Übereinstimmung mit den Sollwerten als die Orbits der Option 1. Bei der anschließenden Berechnung und Betrachtung der Datumsparameter zeigt sich, dass die Jahresamplitude der 11-Satelliten Lösung höher ist als die der 4-Satelliten Lösung. Der mittlere Maßstab der 11-Satelliten Lösung ist 2 mm höher als der der 4-Satelliten Lösung.

Table of contents

1 Introduction

The Earth is always in motion just like its environment (Plag and Pearlman, 2009; Solomon and the Solid Earth Science Working Group, 2002). To describe, understand and visualize the spatial and temporal changes of the Earth system, an International Terrestrial Reference Frame (ITRF) is necessary (GGOS, 2022; Solomon and the Solid Earth Science Working Group, 2002). Movements due to plate tectonics, earthquakes or eruptions, as well as the effects of global climate change such as ice melting and sea level rise can be determined with the help of ITRF (Plag and Pearlman, 2009). In addition, the ITRF is required e.g., for positioning and orbit determination and description of Earth rotation and computation of gravity field models (Plag and Pearlman, 2009).

The accuracy requirement is 1 mm for station positions and 0.1 mm/yr for station motions to monitor accurately the processes described above (Plag and Pearlman, 2009). All techniques used for determining the ITRF must provide their data with the highest possible accuracy to achieve this accuracy for the ITRF solution. The ITRF is computed from the data of the techniques and systems Satellite Laser Ranging (SLR), Very Long Baseline Interferometry (VLBI), Global Navigation Satellite Systems (GNSS) and Doppler Orbitography and Radiopositioning Integrated by Satellites (DORIS) (Plag and Pearlman, 2009).

The SLR technique makes a significant contribution to the ITRF. SLR is responsible for determining the origin of the ITRF. Additionally, SLR defines the scale of the ITRF together with VLBI. This is possible because, with SLR, the distance from a ground station to a satellite can be determined precisely. The measurement accuracy is less than 1 cm (BKG, 2013; Xu, 2010).

However, SLR, like the other techniques mentioned above, is not error-free. Systematic errors in terms of range determination influence the SLR measurements and the geodetic products, like station positions and velocities or Earth Orientation Parameters (EOPs, i.e., polar motion, length-of-day) (Luceri et al., 2019). To account for systematic errors in the ranging data, so-called range biases (RBs) are estimated. Up to the ITRF2014 solution, the range-dependent errors were not treated or only calculated for distinct stations. Nevertheless, they are not negligible. They have a direct influence on the height component of the stations' coordinates (Luceri et al., 2019). The shorter the time period and the smaller the number of observations, the stronger the correlation of the RBs with the respective height component (Luceri et al., 2019). Since the station coordinates are used to realize the scale and the origin of the ITRF further on, the RBs find their way into geodetic products and distort these. The correlation between systematic errors and the altitude component was noticed in 2007 when a new event

timer was installed at the station Herstmonceux (DOMES no. 13212S001, United Kingdom (UK), Code 7840). The altitude component of the station before and after the installation differed by more than 10 mm (Appleby et al., 2008; Appleby et al., 2016).
Furthermore, during the reanalysis of the ITRFs created before 2014, it was noticed that the scales determined with SLR and VLBI differed (Altamimi et al., 2016). To further improve the SLR data, an investigation of the systematic errors and their influence on the EOPs was suggested in 2015 by the International Laser Ranging Service (ILRS) Analysis Standing Committee (ASC). The project is called Systematic System Error Monitoring Pilot Project (SSEM PP). The focus is on the investigation of long-term RBs, as these are representative for measurement stability (Appleby et al., 2016). The SSEM PP took the approach of determining the station coordinates for each station along with the respective RBs.
Appleby et al. (2016) investigated the extent to which the SLR technique and thus RB influence the scale determined by SLR. To achieve this, the RB was estimated for all stations along with orbits, station coordinates, and EOPs. Their investigation showed, through artificially biased data, an impact of not estimated RBs on the station height. A positive RB, which was not observed, leads to a lower station height. With the estimation of RBs, the time series of station heights are less affected. Furthermore, they found that due to systematic errors, the scale of the ITRF has been assumed to be 0.7 ppb too small over the last two decades. The larger scale also reduces the difference to the VLBI scale.
Luceri et al. (2019) obtained a similar result when comparing newly estimated RBs with RBs used within the ITRF2014 processing. In this case, the two scales differed by 1 ppb on average. Due to the positive results, the strategy of SSEM PP was adopted and is currently used for the satellites LAGEOS-1, LAGEOS-2, Etalon-1, and Etalon-2. Only LAGEOS data were used in the Appleby et al. (2016) studies and LAGEOS and Etalon satellites were analyzed in Luceri et al. (2019).
The LAGEOS satellites currently form the basis for ILRS products (Appleby et al.,2016). Their orbits, as well as the satellites themselves, are very well known. The non-gravitational perturbations do not gravely affect their orbits (Strugarek et al., 2021). Both satellites are also observed over a very long time, about 30 years. However, further geodetic satellites are tracked with SLR.

This master thesis is concerned with a computation for long-term mean RBs of SLR observed satellites, whose data is provided by the Deutsches Geodätisches Forschungsinstitut (DGFI-TUM) and will investigate how the additional satellites can improve the scale of the ITRF. The data of following satellites are used: LAGEOS-1/2, Etalon-1/2, Ajisai, Starlette, Stella, WESTPAC 1, Larets, LARES and BLITS. Only for the LAGEOS and Etalon satellites

RBs are currently estimated. For the other seven satellites RBs are estimated in this thesis for the first time.

Figure 1 shows the principle of the estimation of mean RB values. The time series of RBs is examined for periods in which RB values vary around a similar value. In this way, offsets in the time series can be perceived as shown in Figure 1. So, an RB mean value can always be formed to correspond to the course of the RB values.

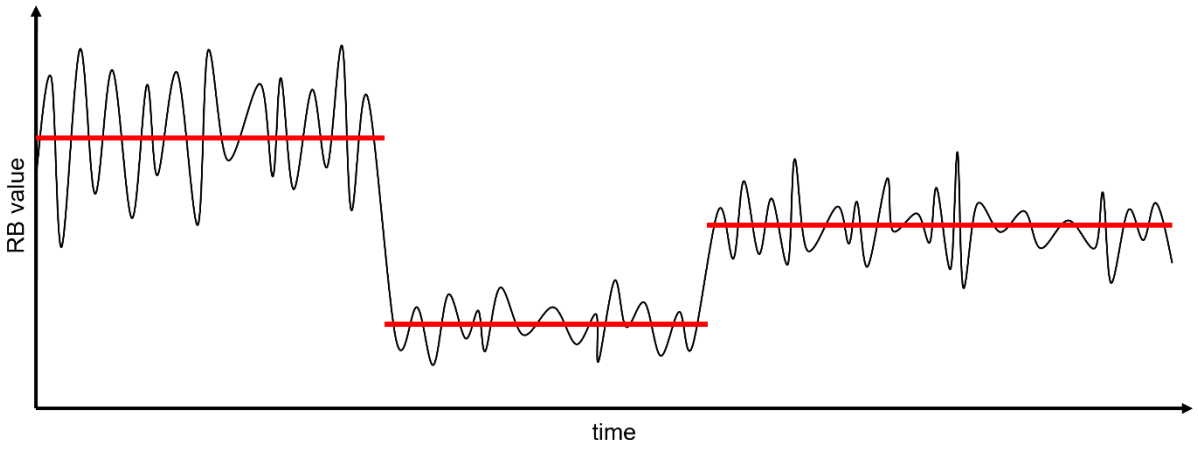

Figure 1: Principle to calculate long-term mean RBs for similarly scattering RB values.

In this thesis different experiments are performed. At first RBs only for the satellite LAGEOS-1 are computed to evaluate the method w.r.t. the official SSEM PP data. In the second step the RBs for all spherical satellites are computed. With the calculated mean RBs the orbits are computed and examined. Finally, the geodetic parameters (the translations in x-, y- and z-direction and the scale), are validated.

The experiments are used to evaluate the research question of this thesis:

Can an 11-satellite solution be used for the ITRF?

In the first part of this thesis the theoretical background of SLR, terrestrial reference frame and precise orbit determination is explained (chapter 2). This is followed by an explanation of the method used to calculate mean RBs (chapter 3). In chapter 4, the results of this thesis are presented and discussed. Finally, a summary and an outlook conclude the thesis.

2 Theory

2.1 Satellite Laser Ranging (SLR)

SLR is next to GNSS, VLBI and DORIS one of the four fundamental geodetic space techniques (Appleby et al., 2016; Rothacher, 2002). It is an optical, 2-way tracking method used to e.g., track Earth orbiting satellites or the Moon (this technique is called Lunar Laser Ranging (LLR)) (Xu, 2010). The determined ranges are required to calculate the orbits of satellites, to obtain and improve coefficients of Earth's gravity field from perturbed orbits, station positions, Earth orientation parameters (EOP) and the Earth's center of mass. Furthermore, together with VLBI it realizes the scale of the ITRF. The ILRS coordinates SLR measurements worldwide (see chapter 2.2). The SLR principle and its challenge factors (influences) are briefly described in the following according to Xu (2010).

The principle of SLR is to measure the runtime of a signal needs between a ground station and a satellite (see Figure 2). For this, a short laser pulse is emitted from the telescope's transmitter to the satellite to be observed. The satellite is equipped with a retroreflector array. The laser pulse is reflected by the retroreflectors of the satellite back to the telescope's receiver. The time between emission and reception of the laser pulse at the ground station is measured. The measured time is called time of flight. Based on the time of flight the range can be calculated.

The basic observation equation for the range ρ is

$$\rho = \left(\frac{\Delta t}{2} * c\right) \tag{2.1}$$

where Δt is the time of flight and c the signal propagation velocity as speed of light in vacuum. The used laser pulse wavelength according to the categorization at DGFI-TUM are 350 nm – 380 nm (ultraviolet light), 420 nm – 430 nm (blue light), 530 nm – 540 nm (green light), 690 nm – 700 nm (old lasers), 845 nm – 855 nm (red light) and 1060 nm – 1070 nm (infrared light) (personal communication DGFI-TUM ILRS AC).

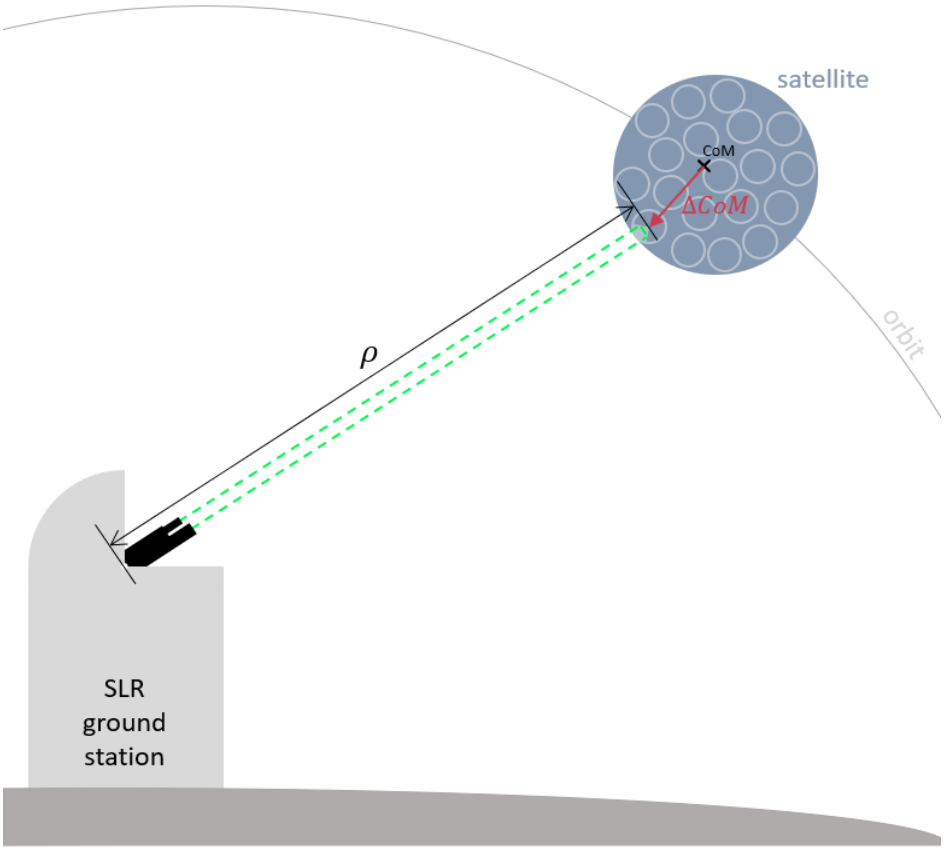

Figure 2: The principle of Satellite Laser Ranging (SLR) (adapted from Seeber,2003 and Xu, 2010)
In green is shown the signal pass. Parallel to the signal the distance ρ is illustrated. CoM shows the center of mass of the satellite.

SLR measurements are not free from external or mechanical influences.

According to Pearlman (1984), there are three categories of errors, which influence the SLR technique:

- **ranging machine errors** as calibration or synchronization problems, mechanical misalignment, hardware malfunctioning or intrinsic device limitations
- **timing errors** as clock offsets
- **modeling errors** as satellite center of mass offsets or force model deficiencies

The first two issues can be actively influenced by conscientious work.

In addition, the correct alignment of the telescope and the reception of a sufficient number of photons is essential. The laser power level and atmospheric conditions must be appropriate to detect a suitable number of photons.

The above mentioned influences also includes the fact that SLR measurements are only possible on cloud-free days. Weather dependency is a disadvantage of SLR technology. Therefore, weather conditions play a role in the selection of station locations. Besides this the

geographical position concerning the global distribution of SLR stations should be considered. The selection of SLR station sites is also influenced by other criteria such as co-location with other geodetic space techniques, a clear horizon for long tracking periods, the geology and security at the site, communication possibilities or the accessibility with respect to the local topography, the infrastructure and the power supply onsite. In addition, the installation and operation of a SLR station is very costly. The operating agency has to afford it to build a SLR telescope, to maintain and operate it. There is a global network of observations stations. Figure 3 shows all locations of SLR stations. It can be seen that the worldwide distribution is not homogeneous as the majority of stations is in the northern hemisphere.

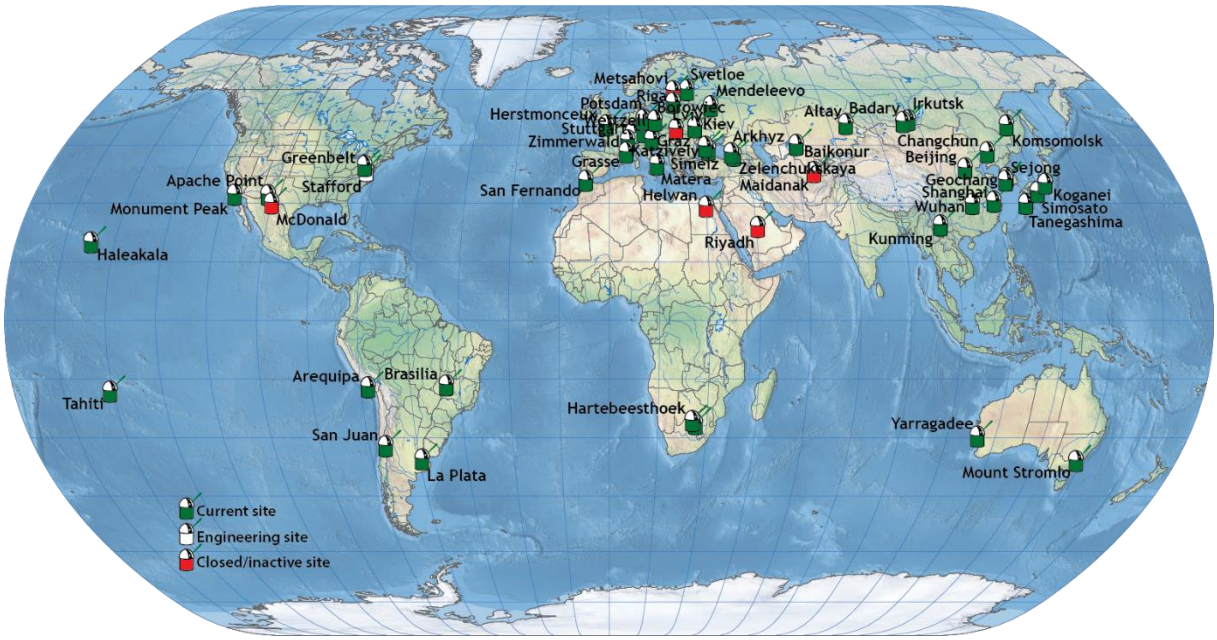

Figure 3: SLR stations of the global ILRS network.[1]

Due to the influences on SLR measurements, the equation of the range (2.1) must be extended in order to improve it and to take influences into account

$$\rho = \left(\frac{\Delta t + TB}{2} * c\right) - a + CoM - RB - GR - \varepsilon \tag{2.2}$$

with

TB	time bias,
a	atmospheric delay correction (due to the troposphere),
CoM	center-of-mass correction,

[1] https://ilrs.gsfc.nasa.gov/network/stations/index.html, last access: 02-16-2022

TB	time bias,
RB	range bias,
GR	relativistic correction,
ε	correction of unknown random errors.

The atmospheric delay correction occurs because the troposphere is dispersive for laser wavelengths and causes a delay of the laser pulse. The mapping function of this effect is optimized for the wavelength of 532 nm in SLR systems. The functions are only applied for elevation angles above 3°.

Besides, there are range and time biases. The time bias is based on the offset between the Coordinated Universal Time (UTC) and the time realized at the station which is in the microsecond range. Furthermore, instrumental phase delays, which are not calibrated, have an impact on the time bias. (Xu, 2010)
Otsubo (2018) defines RBs as constant errors in the range observation. The unit of an RB is meter or millimeter. In other words, if the RB value is positive then the observed distance from the ground station to the satellite is longer than the modelled distance (see Figure 4). In this case, this difference, the RB, must be subtracted. Suppose this is not considered and the RB is not applied, this will falsify the station height in the further calculation of the station coordinates. This establishes the RB as a station dependent error.
Reasons for the bias include errors in the sensors for the barometric pressure, the temperature and the relative humidity and non-linearities in the interval counter. Other reasons for RB in relation to the station are the determined station position in the ITRF, an error in the system delay, an error in the tie between the station coordinate reference point and the SLR telescope reference point or unstable calibration targets. (Xu, 2010)
The reasons in fact need to be further explored because the differentiation between actual physical problems in the measurement system, precision and accuracy of the measurement, shortcomings in the modeling process and statistical correlation may be difficult, since these deviations may be mixing to some degree. (Luceri et al., 2019)
A concrete influence on RBs has the determination of the center of mass (CoM) offset of the respective satellite. The CoM offset value is the difference between the point of reflection of the laser pulse on the retroreflector array and the CoM of the satellite (Luceri et al, 2019). The ILRS suggests the correction of the CoM for geodetic spherical satellites to be calculated on obtainable satellite construction information and properties of the respective ground stations (Otsubo et al., 2015; Luceri et al., 2019).

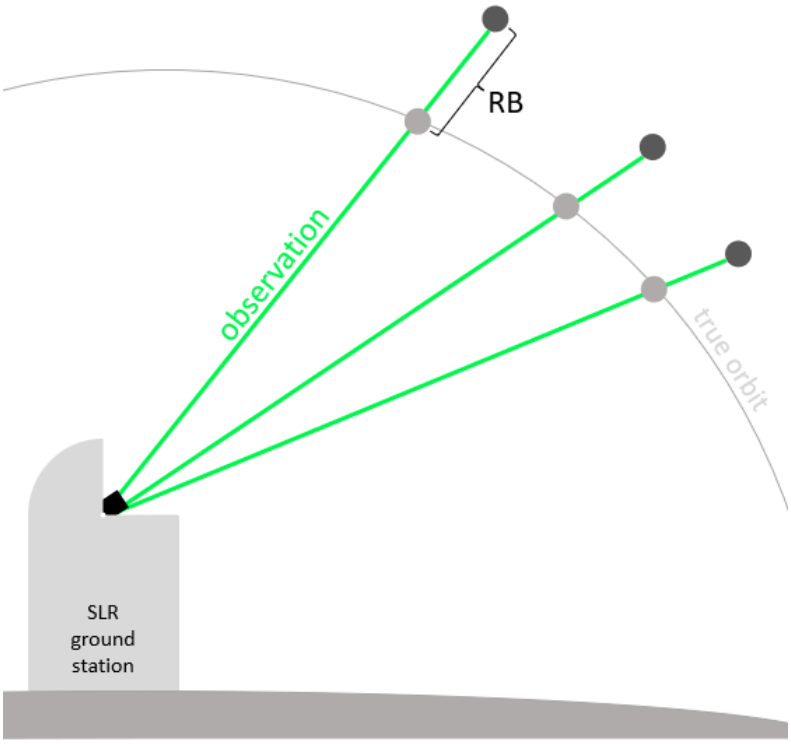

Figure 4:The range bias is the difference between the obtained range to the observed satellite and the actual range to the true orbit (adapted from Otsubo, 2013)

2.2 International Laser Ranging Service (ILRS)

The ILRS is one of the space geodetic services of the International Association of Geodesy (IAG)[2] and hosts one of the Technique Centres of the International Earth Rotation and Reference Systems Service (IERS)[3] . The tasks of the ILRS are collecting, merging, archiving, and distributing of SLR and LLR observation datasets of adequate accuracy (ILRS, 2016). The ILRS promotes the IERS products and scientific research activities such as geodetic and geophysical approaches (ILRS, 2016). The IERS uses the products of the ILRS to provide for example the ITRF, the International Celestial Reference Frame (ICRF) and the EOPs.

The ILRS offers, for example, exact geocentric ground station positions and motions, satellite orbits, Earth's gravity field components and their temporal variations and EOPs (ILRS, 2016). The ILRS coordinates tracking stations, Operations Centres, Data Centres, and Analysis Centres (ACs). The Operation Centres are responsible for collecting and combining the data

[2] https://www.iag-aig.org/services, last access: 22-20-2022
[3] https://www.iers.org/IERS/EN/Organization/About/OrgChart/chart.html, last access: 22-20-2022

from the tracking stations and for executing an initial analysis of data quality besides other tasks. The ILRS Data Centres archive the data and make it available. (ILRS, 2016)
The Analysis Centres are responsible for the quality control. The ACs compute ILRS products using designated standards (ILRS, 2016). The basis for the calculations for the ITRF is the LAGEOS-1 and LAGEOS-2 dataset (ILRS, 2016).
The output of the ACs include weekly averaged station coordinates and satellite orbits as well as daily EOPs for the IERS (ILRS, 2016).

2.3 Systematic System Error Monitoring Pilot Project (SSEM PP)

In the reanalysis of the ITRF2014, it was decided to take a closer look at the scale difference between SLR and VLBI. For many years, the influence of systematic errors in SLR measurements on the ILRS products and thus on the quality of the data has been discussed. Until recently, the full potential of the ILRS Data Handling File (DHF) was not exploited yet, only a few stations with RB were listed and considered in further calculations (see Figure 5).

```
*        1         2         3         4         5         6         7         8
*234567890123456789012345678901234567890123456789012345678901234567890123456789
*--------------------------------------------------------------------------------
+MODEL/RANGE_BIAS
*CODE PT SOLN T START_DATE__ END_DATE____ M __E-VALUE___ STD_DEV _E-RATE__ UNIT   CMNTS
 1874 51   501 A 14:019:00000 20:138:00000 R        -17.8     0.8             mm
 1879 51   501 A 13:188:00000 18:322:00000 R         17.9     1.3             mm
 1887 51   501 A 11:303:00000 15:256:00000 R         21.5     1.8             mm
 1887 51   501 A 16:101:00000 18:343:00000 R        -21.6     1.5             mm
 1890 51   501 A 12:001:00000 21:001:00000 R         12.9     1.1             mm
 1893 51   501 A 05:212:00000 21:001:00000 R        -33.4     1.6             mm
 7080 51   501 A 96:133:00000 01:140:00000 R         -8.4     0.5             mm
 7090 51   501 A 93:001:00000 96:364:00000 R          3.8     0.3             mm
 7090 51   501 A 02:116:00000 10:059:00000 R         -1.7     0.2             mm
 7090 51   501 A 14:208:00000 21:001:00000 R          2.3     0.2             mm
```

Figure 5: Excerpt of the DHF

In 2015, the ILRS ASC initiated the Systematic System Error Monitoring Pilot Project.
The goal was to develop a feasible strategy that could be implemented by all ACs to minimize the RB in the ILRS products or to identify systematic issues (Appleby and Rodríguez, 2015). The developed strategy was a simultaneous dynamic solution, where the station coordinates are estimated together with the RBs (Appleby and Rodríguez, 2015).
Using LAGEOS-1 and LAGEOS-2 data, the weekly coordinates, weekly RBs and daily EOPs should be calculated for each station and satellite from 2005 to 2008 according to the defined strategy. The previously known RBs published in the DHF at that time were not considered in the calculations. As apriori station coordinates, station coordinates from the last realization of

the ITRF were taken. Thereby in each case, the ACs used their own solution strategy considering the ASC standards and the project specifications. (Appleby and Rodríguez, 2015)

The results of the initial analysis of the SSEM PP showed that the ACs could identify RBs in the LAGEOS satellite data. In the comparison of the results of the ACs it was examined whether the found RBs of the ACs per station are in the same order of magnitude. For this purpose, an averaged RB was calculated for each station over the period from 2005 to 2008. The ACs each obtained similar results per station. The SSEM PP shows that it is possible to estimate systematic errors at the millimeter level with its strategy (Appleby and Rodríguez, 2016).
In 2018, in addition to the RBs for the LAGEOS satellites, the RBs for the Etalon-1 and Etalon-2 were determined as part of the SSEM PP. The Etalon satellites were used as a combined solution and not individually. (Pavlis and Luceri, 2018)

2.4 Low Earth Orbit and Medium Earth Orbit satellites

SLR tracks only passive satellites. This means, they receive and reflect a signal coming from the Earth, e.g., laser pulses, but do not transmit any signals themselves. The satellites used in this work are listed in Table 1 and their altitudes and operation periods are shown in Figure 6. The satellites L51 to L54 are Medium Earth Orbit (MEO) satellites since they fly at an altitude of 2000 km and above. They are used for the realization and maintenance of the ITRF and for the monitoring of the deformation of the solid Earth crust and the Earth rotation and polar motion as well as for improving the gravity field model.
The other satellites are Low Earth Orbit (LEO) satellites. They fly at an altitude of 450 km to 1500 km. Starlette is used to monitor the gravity field and to study the main coefficients of the oceanic tides[8]. Stella is used for gravity field recovery[8]. WESTPAC is used to determine stable RBs[9].
All satellites used, have a spherical shape and are equipped with a large number of retroreflectors. All satellites have a nearly circular orbit, except Starlette, which has an eccentric orbit.
The satellite missions BLITS and WESTPAC 1 ended in 2002 and 2013 respectively[10]. All other missions are still ongoing[4].

Table 1: Central mission parameters of the used spherical LEO and MEO satellites (SP3c code: Code of Extended Standard Product 3 Orbit Format).]

Satellite	SP3c code[4]	Launch date [mm-dd-yyyy]	Last data date [mm-dd-yyyy]	Altitude [km]	Inclination [degrees]	Eccentricity
Ajisai[5]	L50	08-12-1986	-	1,490	50.0	0.001
LAGEOS-1[6]	L51	05-04-1976	-	5,860	109.84	0.0045
LAGEOS-2[6]	L52	10-22-1992	-	5,620	52.64	0.0135
Etalon-1[7]	L53	01-10-1989	-	19,120	64.9	0.00061
Etalon-2[7]	L54	05-31-1989	-	19,120	65.5	0.00066
Starlette[8]	L55	02-06-1975	-	812 - 1114	48.83	0.0206
Stella[8]	L56	09-26-1993	-	804	98.6	0.001
WESTPAC 1[9]	L58	07-10-1998	01-12-2002[10]	835	98	0.0
Larets[11]	L59	09-27-2003	-	691	98.204	0.0002
BLITS[12]	L60	09-17-2009	03-05-2013[10]	832	98.77	ca. 0.0015[13]
LARES[14]	L61	02-13-2012	-	1450	69.5	0.0

[4] https://cddis.nasa.gov/sp3c_satlist.html, last access: 03-10-2022
[5] https://ilrs.gsfc.nasa.gov/missions/satellite_missions/current_missions/ajis_general.html, last access: 03-10-2022
[6] https://ilrs.gsfc.nasa.gov/missions/satellite_missions/current_missions/lag1_general.html, last access: 03-10-2022
[7] https://ilrs.gsfc.nasa.gov/missions/satellite_missions/current_missions/eta1_general.html, last access: 03-10-2022
[8] https://ilrs.gsfc.nasa.gov/missions/satellite_missions/current_missions/star_general.html, last access: 03-10-2022
[9] https://ilrs.gsfc.nasa.gov/missions/satellite_missions/past_missions/west_general.html, last access: 03-10-2022
[10] https://ilrs.gsfc.nasa.gov/missions/satellite_missions/past_missions/index.html, last access: 03-10-2022
[11] https://ilrs.gsfc.nasa.gov/missions/satellite_missions/current_missions/lare_general.html, last access: 03-10-2022
[12] https://ilrs.gsfc.nasa.gov/missions/satellite_missions/future_missions/bltm_general.html, last access: 03-10-2022
[13] DGFI-TUM
[14]https://ilrs.gsfc.nasa.gov/missions/satellite_missions/current_missions/lars_general.html , last access: 03-10-2022

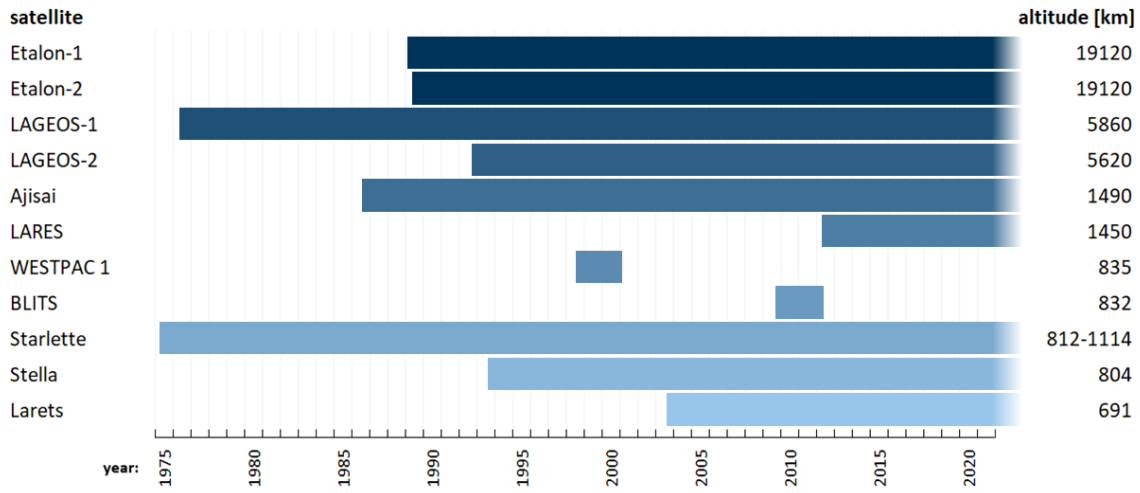

Figure 6: Operation periods and altitudes of the used satellites

2.5 Satellite Orbit Perturbations

For the calculation of ILRS products, like the determination of the origin of the ITRF, the orbits of the observed satellites have to be computed accurately. The accurate orbit calculation must consider the perturbations acting on the satellite, which is briefly discussed below according to Xu (2010) and Doornbos (2012).

In a first approximation, a satellite's motion is considered a two-body problem. The acceleration acting on a satellite can be expressed by Newton's law of gravity, assuming that the earth is spherical

$$\ddot{\boldsymbol{r}} = -\frac{GM_{\oplus}}{r^3}\boldsymbol{r} \tag{2.3}$$

with

$\ddot{\boldsymbol{r}}$ acceleration in a geodetic reference frame,

$GM_{\oplus}$ product of Earth's gravitational constant and its mass,

r geocentric range (given by $\sqrt{(\boldsymbol{r} * \boldsymbol{r})}$),

$\boldsymbol{r}$ position vector of the satellite.

However, the formula must be extended because the Earth is not spherical and various forces act on the satellite. These forces must be modeled and applied when calculating the acceleration

$$\ddot{\boldsymbol{r}} = -\frac{GM_{\oplus}}{r^3}\boldsymbol{r} + \boldsymbol{f} \tag{2.4}$$

Since several forces act on the satellite, the applied force $\boldsymbol{f}$ is composed of different forces

$$\boldsymbol{f} = \boldsymbol{f_{NS}} + \boldsymbol{f_{TC}} + \boldsymbol{f_{3B}} + \boldsymbol{f_g} + \boldsymbol{f_{Drag}} + \boldsymbol{f_{SRP}} + \boldsymbol{f_{ERP}} + \boldsymbol{f_{other}} + \boldsymbol{f_{Emp}} \tag{2.5}$$

with

$\boldsymbol{f_{NS}}$	effects due to uneven Earth's mass distribution
$\boldsymbol{f_{TC}}$	effects of the temporal variations of the Earth's gravity field
$\boldsymbol{f_{3B}}$	effects of the gravity of third bodies such as the Sun, the Moon and planets
$\boldsymbol{f_g}$	effects of general relativity
$\boldsymbol{f_{Drag}}$	effects of the atmospheric drag
$\boldsymbol{f_{SRP}}$	effects of solar radiation pressure
$\boldsymbol{f_{ERP}}$	effects of Earth albedo reflectivity and infrared emissivity radiation pressure
$\boldsymbol{f_{other}}$	effects of other forces
$\boldsymbol{f_{Emp}}$	empirical corrections

The forces consist of gravitational and non-gravitational forces.

The gravitational forces are caused by the Earth's gravity field. The Earth's gravity field depends on the mass distribution on the Earth's crust, in the Earth's fluid envelope and in the Earth's interior and the centrifugal acceleration due to the Earth's rotation. As mentioned above the Earth is not spherical, the Earth is slightly flattened due to the Earth's rotation. This also has an effect on the Earth's gravity field. (Seeber, 2003)

In addition, the Earth's gravity field does not only change due to the motions of the Earth, also the Sun and the Moon act on the Earth's gravity field with their gravitational forces. The effects of the Sun and the Moon show up as, e.g., Earth's tides, ocean tides and pole tides. These occur periodically due to the Earth's rotation.

The gravitational forces of the Sun and the Moon, together with the gravitational forces of planets, also lead to an acceleration and a deceleration of the satellite. The gravitational impacts have a more decisive influence the higher the altitude is.

In addition, the effects of general relativity also belong to the gravitational forces.

The non-gravitational forces depend on the surface of the satellite next to the altitude. One non-gravitational force is the atmospheric drag. This effect is part of the aerodynamic accelerations. The lift and side forces can be neglected for spherical satellites due to the symmetric shape of the satellite (Doornbos, 2012). The force acts in the opposite direction to the relative motion of the satellite with respect to the surrounding atmosphere. Therefore, the satellite's velocity is slowed down. This effect is significant for LEO satellites. (Xu, 2010)

Furthermore, the acceleration due to solar radiation belongs to the non-gravitational forces, as well as the acceleration due to Earth's radiation. The satellite's acceleration comes from the absorption and reflection of the radiation on the satellite. The Sun is the primary radiation source and has a more significant influence with increasing altitude. The solar radiation can act from different directions on the satellite (Doornbos, 2012). However, the Earth's radiation also affects the satellite. This force only acts in the radial direction on the satellite (Doornbos, 2012). However, the Earth's radiation also affects the satellite. The Earth's radiation comprises reflected solar radiation and outgoing longwave radiation. The reflected solar radiation is also called albedo, which describes the part of the incoming light reflected back, while the outgoing longwave radiation includes infrared radiation. The albedo value depends on the reflecting surface. For example, the value for soil and vegetation-covered surfaces is on average 0.05 and for snow, ice or clouds 0.8. The Earth's albedo is approximately 0.3 (Wertz, 1978). The part of the received sunlight not directly reflected is absorbed and converted into heat. This heat is re-radiated and is called infrared radiation. The infrared radiation is lower for brighter surfaces because these reflect much solar radiation and absorb less energy (Wertz, 1978).

Among the empirical forces, parameters can be modeled as once per revolution accelerations, representing very small previously unmodelled forces. They are implicated by the radial, tangential and normal components (Xu, 2010).

The other forces mentioned in the equation can be, e.g., effects of the Earth's magnetic field (like the South Atlantic Anomaly[15]). Other forces are thermal effects or thruster accelerators (Xu, 2010).

[15] https://www.nasa.gov/feature/nasa-researchers-track-slowly-splitting-dent-in-earth-s-magnetic-field, last access: 03-10-2022

2.6 International Terrestrial Reference Frame (ITRF)

The ITRF is the realization of the International Terrestrial Reference System (ITRS). The ITRS is the theoretical definition of a reference system. The definition is defined in the IERS Conventions (Petit and Luzum, 2010).

The ILRS as well as its realization is defined as a trihedron in the three-dimensional Euclidean vector space (Figure 7). The three vectors are orthogonal to each other and form a right-handed system. The system rotates with the earth and is geocentric. Therefore, the reference system originates in the CoM of the Earth. The orientation is equatorial. Accordingly, two axes lie in the equatorial plane. The X-axis passes through the Greenwich meridian. The Z-axis points towards the North Pole. (Petit and Luzum, 2010)

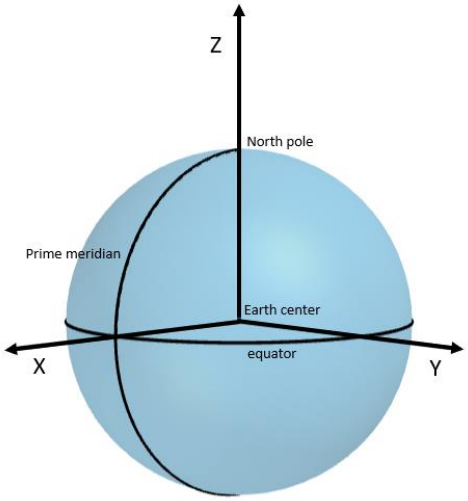

Figure 7: Coordinate System of the International Terrestrial Reference System and its realization (adapted from Seeber, 2003).

The ITRS is realized by three-dimensional coordinates and velocities, as well as EOPs. In each case, the coordinates refer to fixed points on the Earth's crust.

The ITRF is calculated by combining the data of the four geodetic techniques: SLR, VLBI, GNSS and DORIS. By combining the techniques, more observations are available, and the techniques can compensate the disadvantages of each other. Thus, for example DORIS is globally homogeneous distributed in contrast to SLR. GNSS provides a huge number of stations due to the easy handling and VLBI allows the determination of all EOPs.

Three IERS Combination Centres[16] (CC) calculate the ITRF solutions: Institut National de l'Information Géographique et Forestière (IGN), Deutsches Geodätisches Forschungsinstitut

[16] https://www.iers.org/IERS/EN/Organization/ITRSCombinationCentres/ITRSCC.html, last access: 03-02-2022

(DGFI-TUM), Jet Propulsion Laboratory (JPL). Each CC follows a different strategy in the realization of the ITRS.

At DGFI-TUM, data and techniques are combined at the normal equation level of the Gauß-Markov model. The software DGFI Orbit and Geodetic Parameter Estimation Software with the module Combination and Solution (DOGS-CS) is used for this purpose. (Bloßfeld, 2015)

Due to the dynamics of the Earth the IERS publishes every three to six years a new ITRF. On this occasion new stations can be included and the ITRF will refer to the current time series of measurements. The latest publication is the ITRF2014. The ITRF solution of the DGFI-TUM is called DTRF2014.

3 Methodology

For each station that observed the satellites listed in chapter 2.4, long-term mean RBs are computed by using the software MATLAB. The long-term RBs are generated by calculating weighted mean values over a time period defined previously. Two options are calculated, which differ mainly due to their number of used stations. For each option the weighted mean RBs are determined using the weekly RBs calculated in the 4-satellite solution (LAGEOS-1/2, Etalon-1/2) and using the weekly RBs calculated in the 11-satellite solution (consisting of all satellites named in Table 1, see chapter 2.4).
In chapter 3.1, the input data are described. The computation approach is specified in chapter 3.2.

3.1 Input data

The input data are weekly solutions of the RBs for the stations, which observed the 11 satellites Ajisai, LAGEOS-1/2, Etalon-1/2, Starlette, Stella, WESTPAC 1, Larets, LARES and BLITS. They are provided by the ILRS AC DGFI-TUM and will in the following be referred to as the 11-satellite solution. Additionally, in order to validate the calculation method of the mean RBs, the weekly solutions using LAGEOS-1/2 and Etalon-1/2 observations have been computed and provided by the ILRS AC hosted at DGFI-TUM. This is nearly the official ILRSA solution (official primary ILRS combination) and will be referred to as the 4-satellite solution.
In this thesis, the weekly solutions from 1993 to 2020 are used respectively for the 4- and the 11-satellite solution. The input data contains the DOMES numbers (Directory of MERIT Sites, DOMES no.) of the stations, the time in relation to the epoch J2000.0[17], the respective satellite number, the estimated value, the deviation from the apriori value, the associated standard deviation and the number of observations that were included in the estimation. For Etalon-1 and Etalon-2 a combined solution (LEC, Etalon Combined) of the weekly solutions was available and used.
For further calculations the weekly solutions were sorted by satellites respectively for the 4- and the 11-satellite solution. Each file contains all stations that have observed this satellite. For the Etalon satellites, only stations that observed at least one other satellite in the respective week are included in the weekly solution.

[17] J2000.0 = JD 2451545.0 = January 1, 2000 12^h 0^m 0^s TDB = January 1, 2000, 11^h 58^m 555.816^s UTC (TDB = Barycentric Dynamical Time; UTC = Coordinated Universal Time (Seidelmann, 1992)

3.2 Data evaluation

Station selection

Before calculating the respective weighted mean values of an observing SLR station, on the one hand the SLR stations useful for this study are selected and on the other hand the time series of the RBs of the selected SLR stations are checked for outliers.

Firstly, the observation stations and their performance are determined for each satellite. The total number of observation times for each SLR station is identified, which corresponds to the number of available RBs of the respective SLR station. Furthermore, the number of observations included in the calculation of the RBs and the time span over which the station has repeatedly observed the satellite (in days and years) is determined.

Based on the fact, that a maximum of 52 weekly solutions can be available within one year and that an observation period of less than one year does not lead to a meaningful result of a mean RB value, all stations with less than 52 RBs are removed.

$$used\ stations = n_{Stations}(n_{RB} > 52) \tag{3.1}$$

with

$n_{Stations}$ number of stations observing considered satellite,

n_{RB} number of RB values at the considered station.

These selected stations are used for option 1 (see Table 2).

Option 2 takes a closer look on the performance of the individual stations. The stations differ in the spread of respective RB values, in possible data offsets and data gaps. With option 2, only mean RB values for stable measuring stations are calculated. This has the consequence that, in option 2, fewer stations are taken into account in total. For the selection of stations for option 2, a minimum observation period of 4 years was considered based on the selected stations of option 1, as well as the number of RBs per year and the number of observations per year (see formula 3.2 and 3.3). Over 4 years, a station should have measured regularly and a certain stability in the values should be present that a suitable mean value can be calculated.

$$RB\ per\ year = \frac{n_{RB}}{t_{End} - t_{Start}} \tag{3.2}$$

$$observations\ per\ year = \frac{n_{obs}}{t_{End} - t_{Start}} \tag{3.3}$$

with

n_{obs} number of observations at the considered station,

t_{Start} year of the first RB of the considered station,

t_{End} year of the last RB of the considered station.

To discuss whether the number of stations for which mean RBs are calculated has an influence on the further analysis, the mean RB calculation is performed for two options (see Table 2) respectively for the 4- and 11-satellite solution.

Table 2: Station selection options and their criteria.

	number of weekly solutions (formula 3.1)	number of observing years	Number of RB/year (formula 3.2)	Number of observations/year (formula 3.3)
Option 1	> 52	> 1 yr	-	-
Option 2	> 52	> 4 yr	calculated	calculated

Outlier detection

The next step is carried out equally for all stations. Here, the remaining stations are checked for possible outliers. An outlier is defined as a value that varies widely from the surrounding values. Outliers should not play a role in the mean value calculation since they can significantly influence the respective mean value. In addition, it cannot be assumed that the outliers have explicitly a high standard deviation. Therefore, outliers are not always down weighted and consequently have less impact on the mean value. It should be distinguished whether the deviating value is an erroneous measurement (rough error) that can be discarded or whether the value represents an exceptional event, which must be considered separately. The station history logs[18] can be helpful but not all stations have a history log on a similar level of detail. Therefore, the outliers are determined as described in the following.

Since in the ideal case there are no systematic errors in the observations, the expected value of the RBs is set to zero. Whereas the RB values of the stations are assumed to be normally distributed due to the large amount of data, it is assumed that 99.7% (=3σ) of the data fit each other to the expected value of 0 (see Figure 8). For LAGEOS-1 this assumption results in a

[18] https://edc.dgfi.tum.de/en/stations/ last access: 03-22-2022

range of values from -0.12 m to +0.12 m for all available data (see Figure 8). For option 2 this assumption was applied (see Table 4).

Using random sampling for LAGEOS-1 and Etalon-1 for option 1, these thresholds were found to be too low as too many values were discarded. Thus, the value ±0.15 m was set as the new threshold for option 1.

However, there is still a possibility that stations showing RB time series shifted by an offset of up to 0.1m (e.g., station 12205S001, Borowiec, Poland). Therefore, it must be ensured that also these RB time series scattering around an offset unequal to zero must be taken into account in the calculations and must not be marked blanketly as outliers even if they are located outside the favored value range. The values defined as outliers are analyzed in a multi-step procedure to avoid this.

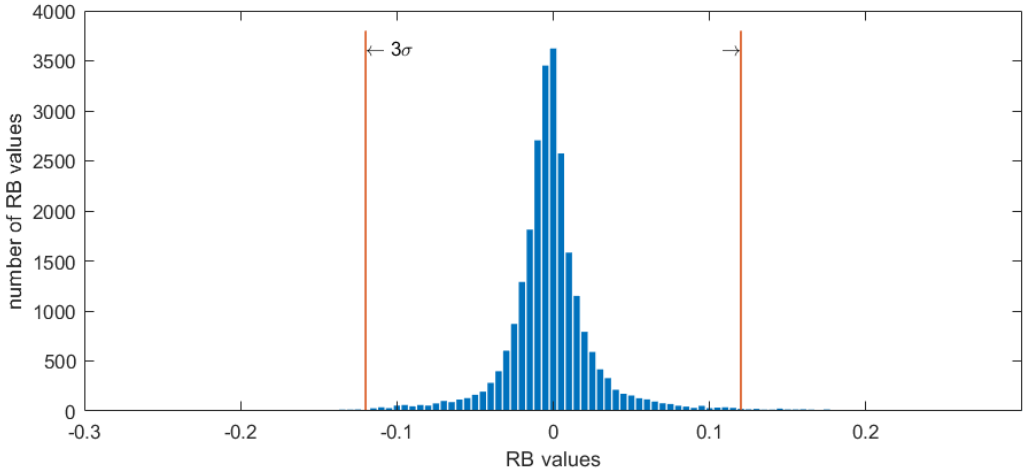

Figure 8: Histogram of all LAGEOS-1 data of all stations of the 4-satellite solution. The red lines show the outlier thresholds at ±0.12 m of option 2.

Outlier post-processing

All values smaller than the negative outlier threshold (-0.15 m for option 1; -0.12 m for option 2) and larger than the positive outlier threshold (+0.15 m for option 1; +0.12 m for option 2) are considered for the mean RB computation.

In the following, the extent to which outliers really represent individual values that do not match the surrounding RB values is evaluated (see Figure 9). In order to assess the respective influence of the outliers on the data set, the percentage ratio of the outliers on the entire data set of a station is calculated. Based on a differentiated analysis of a sample of stations, it could be said that detected outliers with a percentage ratio smaller than 5% are outliers by definition. So, these detected outliers are not to be considered in the further calculation. The threshold value is set to 5%. This means that if the ratio of detected outliers to all RBs of one station is only up to 5%, then these outliers are marked to be deleted for the mean calculation.

$$deleted\ outliers = detected\ outliers\left(\frac{n_{out}}{n_{RB}} < 5\%\right) \tag{3.4}$$

with

n_{out} number of outliers at the considered station

If more than 5% of the values in a data set are detected as outliers, it must be assumed that the outliers occur frequently or have a large influence on the entire data set. Thus, if the ratio of detected outliers is greater than 5 %, these outliers are analyzed further. In this case, all outliers and their influence on the data collected in the same year are considered separately. For further steps, the number of detected outliers is analyzed. If there are one or two outliers per year, they are examined separately. If there are three or more outliers per year, the percentage of the outliers in the respective year is considered as:

$$outliers\ in\ respective\ year\ [\%] = \frac{n_{out,yr}}{n_{RB,yr}} \tag{3.5}$$

with

$n_{out,yr}$ number of outliers in respective year,

$n_{RB,yr}$ number of RBs in respective year.

The larger the percentage (> 50%) and thus the influence of the outliers, the more likely the data must remain in the data set. If the proportion is smaller, a comparison is made of how well the outliers within a year match each other or how well they match existing outliers in the year before or after. If there are several outliers (two and more) in one year and they fit well to each other, i.e., the difference is smaller than 0.1 m, the values remain in the data set. The threshold of 0.1 m is chosen visually.
Multiple outliers present in one year can either vary strongly or all lay outside the predefined data interval and thus represent an offset of the mean. They should not vary further than the one-sided outlier threshold (0.15 m (option 1); 0.12 m (option 2)) in order to enable a representative mean value. Hence, the deviation of the outliers should be smaller than 0.1 m (e.g., station 12340S002, Maidanak 1, Uzbekistan) The aim is to reassess the data without losing too much information.

In the other case, that the outliers differ strongly within one year, the percentage of the mean value of all outliers in this year on the mean value of all data within this year is considered:

$$ratio\ of\ outliers\ on\ mean\ of\ respective\ year[\%] = \frac{\left(\frac{\sum_{j=1}^{n_{out,yr}} x_{out\,j}}{n_{out,yr}}\right)}{\left(\frac{\sum_{i=1}^{n_{RB,yr}} x_i}{n_{RB,yr}}\right)} \quad (3.6)$$

with

x_{out} RB value of an outlier,

x RB value.

If the influence of individual values on the mean value of a specific year is high, they fit the definition of an outlier and should not be considered in the following calculation to avoid any distortion. In the other case, if the influence is small, the outliers can remain in the data set.
The additional analysis of these cases in a sample of stations revealed that if the influence of the outliers on the mean value was more than 20%, at least one of the outliers considered was an outlier in the sense of the definition and should be neglected. Hence, the outlier with the highest value is marked to be deleted, if the influence is greater than 20 %. Otherwise, the value remains in the data set.

In the case of only one outlier in one year, it is examined, whether there is also an outlier in the year before or after. If the outlier found is the only outlier within three years, a distinction is made between how many weekly RBs are available within the respective year. If there are more than two values, the outlier is dropped from the data set, because the percentage of the outlier on all data of the year is less than 50 %. However, if the percentage is greater than 50 %, the value is an outlier that remains in the data set and should be considered separately.

After all values smaller or larger than the basic threshold for outliers, e.g., ±0.15 m, have been considered, the values marked to be deleted for further calculations are finally checked (see Figure 9). In the case of two outliers within one year, the difference of the two outliers to each other as well as the difference to the neighboring outliers is considered. Furthermore, it is tested whether the minimum or maximum value of an outlier remaining in the data set lies in the year before or after the outlier to be checked and whether the outlier to be checked is larger or smaller than the value of the accepted outlier. In addition, it is examined whether the difference between the outlier and the minimum or maximum value within the year is less than 0.05 m. If the above cases apply, the outlier remains in the data set, otherwise, it is finally dropped from the further calculation.

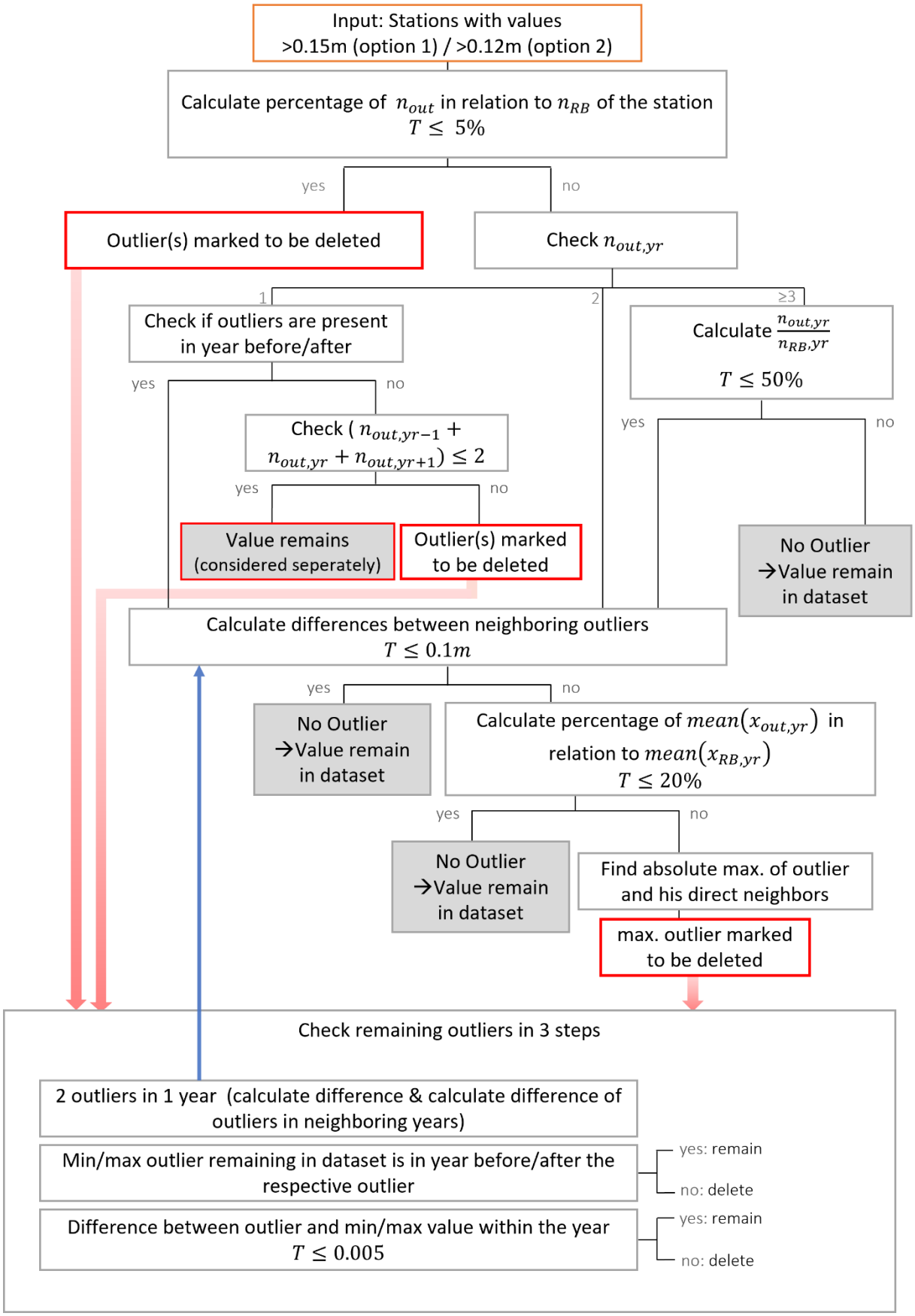

Figure 9: Flow chart of the determination of outliers.
The white boxes show the calculation steps; the grey boxes show the detected outliers, which remain in the dataset (no outliers); the red boxes present the detected possible outliers and have to be checked again in the end before deleting; The grey box with the red outline represents detected outliers, which are the only values in a station time period of 3 years. These values have to be considered separately in step 5 of the determination of time periods (see Figure 10 and Figure 11)

Mean calculation

The arithmetic mean $\bar{x}$ is defined as

$$\bar{x} = \frac{1}{n}\sum_{i=1}^{n} x_i \tag{3.7}$$

with

$\bar{x}$ arithmetic mean,

x_i i-th RB value,

n number of RB.

Because the given RBs are based on a different number of observations, the RBs cannot be treated equally in the calculation. So, the mean value is calculated as weighted arithmetic mean $\bar{x}_w$:

$$\bar{x}_w = \frac{\sum_{i=1}^{n} w_i x_i}{\sum_{i=1}^{n} w_i}\ , \tag{3.8}$$

with

$\bar{x}_w$ weighted arithmetic mean,

w_i i-th weight.

The used weights are the variances calculated from the standard deviations given for each RB in the input data. To increase the weighting of the i-th RB calculated by a large number of observations compared to an RB estimated from a small number of observations, the inverse value of the variance σ_i^2 is used:

$$w_i = \frac{1}{{\sigma_i}^2} \tag{3.9}$$

So, the mean value of the RB is calculated as inverse-variance weighted average $\hat{x}_w$:

$$\bar{x}_w = \hat{x}_w = \frac{\sum_{i=1}^{n} \frac{x_i}{\sigma_i^2}}{\sum_{i=1}^{n} \frac{1}{\sigma_i^2}} \tag{3.10}$$

In the following, the inverse-variance weighted average is called mean or weighted mean.

To evaluate the significance of the weighted mean values of the RBs, the corresponding standard deviation σ_w and the weighted root mean square (RMS) value x_{RMS_w} are calculated:

$$\sigma_w = \sqrt{\frac{\sum_{i=1}^{n}\left(\frac{x_i - \bar{x}_w}{\sigma}\right)^2}{\sum_{i=1}^{n}\left(\frac{n-1}{\sigma^2}\right)}} \tag{3.11}$$

$$x_{RMS_w} = \sqrt{\frac{\sum_{i=1}^{n}\left(\frac{x_i - \bar{x}_w}{\sigma}\right)^2}{\sum_{i=1}^{n}\frac{1}{\sigma^2}}} \tag{3.12}$$

Determination of periods

After removing erroneous data, the data sets of each station are divided according to the wavelength used for the observation. A distinction is made between the wavelengths of green, red, blue and infrared light (for the wavelength ranges see chapter 2.1). All stations observed satellites with a wavelength in the green spectrum. The SLR stations Zimmerwald (DOMES no. 14001S007, Switzerland) and Conception (DOMES no. 41719M001, Chile) also used other wavelengths (colors) mentioned above.

The weighted mean values of the RBs, which show a similar scattering, are calculated in six steps for each station. Mean values are to be determined over the longest possible time periods, in which the scattering of the respective RBs is similar. The longer the time period the more the mean value tends towards zero, presuming the values scatter around zero. With long time periods, changes in the course of the data are perceived less well or not at all. In order to perceive changes in the data set as best as possible, a short period of one year is selected at the beginning of the computation (see Figure 10).

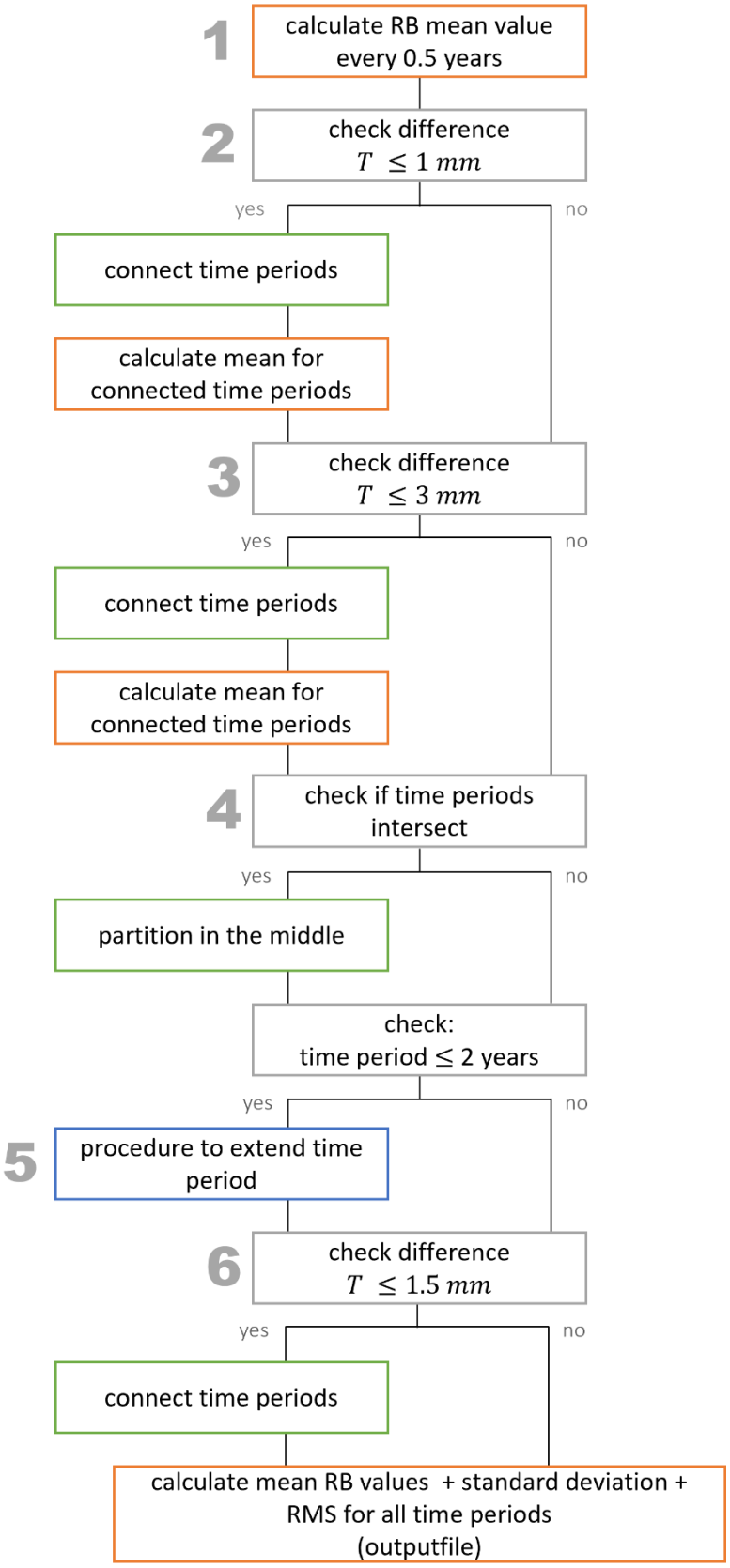

Figure 10: Flow chart of the determination of time periods with similar varying RB values.
In the orange blocks, the calculation parts are represented; the green blocks show the parts in which time periods are connected or partitioned; grey blocks present the parts in which the RB values or the time periods are checked; the blue block (step 5) refers to Figure 11.

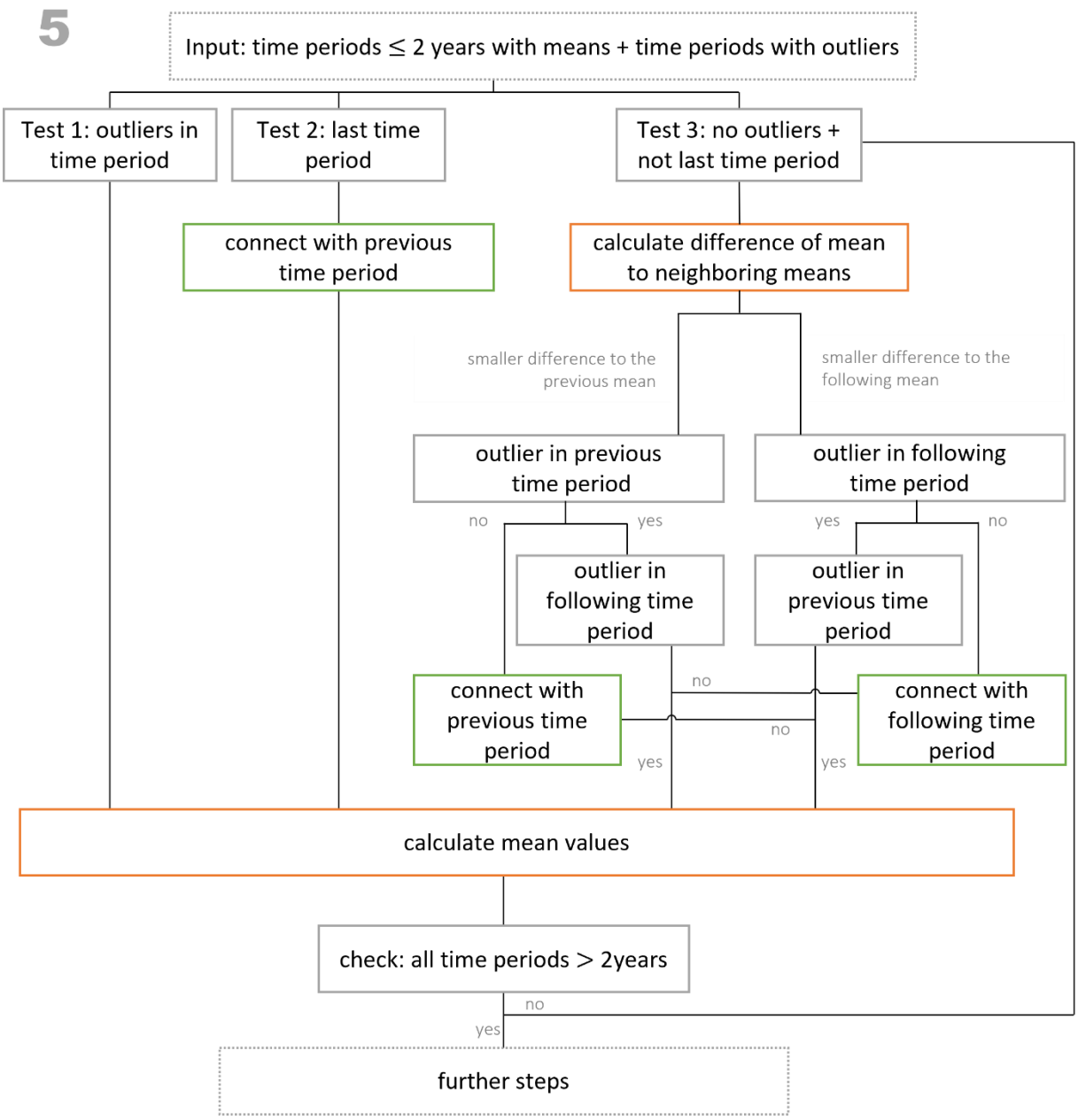

Figure 11: Step 5 of the determination of time periods (see Figure 10). The steps to extend time periods ≤ 2 years are shown. In the orange blocks the calculation parts are represented; the green blocks show the parts in which time periods are connected or partitioned; the grey blocks present the parts in which the RB values or the time periods are checked; the grey dotted blocks show the input to perform step 5 and the reference to the following steps (see Figure 10).

In the first step (see Figure 10), mean values are calculated for a moving one-year window with a time step of half a year, e.g., 2000-2001, 2000.5-2001.5, 2001-2002, etc. No mean values are calculated without any weekly RBs estimated.

In the second and third steps (see Figure 10), the time periods are slowly enlarged by linking time periods whose mean values have a small difference. First, very well matching time periods with a mean value difference of 1 mm are equalized. After a renewed weighted mean value

calculation, time sections are linked together whose mean value difference is less than or equal to 3 mm.

Then it is checked whether there are still overlapping time periods (step 4). If this is the case, the overlapping period of half a year is divided in the middle. This results in minimum time sections of half a year.

In order to obtain time periods longer than two years, sections shorter or equal two years are added to the next matching section in the 5th step (see Figure 11). The minimal observation time of a station for LAGEOS-1 is two years in option 1 (e.g., station 14001S001 (Zimmerwald, Switzerland) with 2.2 years). For all included stations in option 2, the selected time period of two years is the half of the defined minimal total observation time (> 4 yr). A check is made to detect the difference between the time period to be examined and the previous or next time period. The time sections with the smaller difference are equalized. If there is an outlier in one of the considered time periods defined at the beginning to be handled separately, this time period is not added to any other time period and no time period is added to this time period.

In addition, if the mean value calculated over the first or last years in the data set differ by more than 0.02 m from the next or previous calculated mean value, these time periods are considered separately and retain their own mean value regardless of whether the time period is shorter than two years. The value 0.02 m is the smallest difference, which is perceived in good performing stations like Herstmonceux (DOMES no. 13212S001, UK, CDP Pad ID 7840) or Yarragadee (DOMES no. 50107M001, Australia, CDP Pad ID 7090). These stations have a smooth and long time series of weekly RBs due to long observation times under good conditions as day and night observations, use of up-to-date technology.

The last step (step 6) checks once again whether successive mean values have a small difference of less or equal to 1.5 mm. If this is the case, the time period is increased over the time span of the two mean values. Finally, time intervals are obtained with a minimum length of two years and, in exceptions, are between 0.5 and 1.75 years long.

Output file

The weighted mean, the standard deviation and the RMS value for each of these periods are calculated by the defined time periods.

Each output file contains for every single calculated weighted mean the Station Identification number (ID), the code for the satellite, the wavelength, start and end time for the time period in which the RB applies, the weighted mean value and the related standard deviation value in millimeters.

The calculated weighted means for each station per satellite and wavelength are fed into DOGS-CS. All parameters corresponding to the DTRF2020 are unchanged (for the detailed

parameters see Bloßfeld et al., 2020). For all stations not mentioned in the output file no RB is estimated in the further calculations.

4 Analysis and Discussion

4.1 Overview of provided data and computed solutions

Table 3 shows all processing options used for the analysis:

Table 3: Processing options used in the analysis for this thesis

			Data basis	**LAGEOS-1/2 Etalon-1/2**	**Ajisai, Starlette, Stella, WESTPAC 1, Larets, LARES, BLITS**
Provided data	Mean RBs	**DTRF2020 (4 satellites, SSEM PP)**	ASI CC	X	-
	Weekly RBs	**Reprocessed data** (4 satellites, settings similar to SSEM PP)	DGFI-TUM	X	-
	Weekly RBs	**Reprocessed data** (11 satellites, settings similar to SSEM PP)	DGFI-TUM	X	X
Computed solutions	Mean RBs	**Option 1: 4 satellites**	DGFI-TUM	X	-
		Option 1: 11 satellites	DGFI-TUM	X	X
		Option 2: 4 satellites	DGFI-TUM	X	-
		Option 2: 11 satellites	DGFI-TUM	X	X

The DTRF2020 data include the mean RBs from the ILRS DHF (version of 04-16-2021, personal communication DGFI-TUM ILRS AC) for the LAGEOS and Etalon satellites. The mean RBs values in the DHF are based on the combination of mean RBs from different ACs at the ILRS CC hosted by the Italian Space Agency (Agenzia Spaziale Italiana, ASI).
The reprocessed data of the 4-satellite solution contains the weekly solutions of the LAGEOS and Etalon satellites. These data are the input of the DGFI-TUM ILRS AC to the SSEM PP.
For the reprocessed data of the 11-satellite solution, the weekly RBs for all 11 satellites were calculated using the SSEM PP method. These weekly values were used to calculate the mean RBs of the 11-satellite solution. The 11-satellite solution enables, by the different inclinations of used satellites, a decorrelation of the orbit parameters (e.g., solar radiation pressure scaling factor or the empirical acceleration amplitudes) (Bloßfeld et al., 2018).

For the analysis four further options have been computed. The mean RBs of these options were determined as part of this thesis. Options 1 and 2 were applied to the 4- and 11-satellite solutions. The different parameters included in the respective options in the analysis of the data and the calculation of the mean values can be seen in Table 4. The options differ due to the selection of stations (see chapter 3.2), while the 4- and 11-satellite solutions differ due to the number of satellites and observations used to compute the weekly RB solutions.

Table 4: The criteria of the options for those stations long-term mean RBs are calculated

	abbreviation	number of satellites	minimal total observation time (see Table 2)	consideration of i.a. RB per year (see Table 2)	outlier threshold
Option 1: 4 satellites	O1-4	4	> 1yr	-	±0.15 m
Option 1: 11 satellites	O1-11	11	> 1 yr	-	±0.15 m
Option 2: 4 satellites	O2-4	4	> 4 yr	X	±0.12 m
Option 2: 11 satellites	O2-11	11	> 4 yr	X	±0.15 m

4.2 4-satellite solution and 11-satellite solution

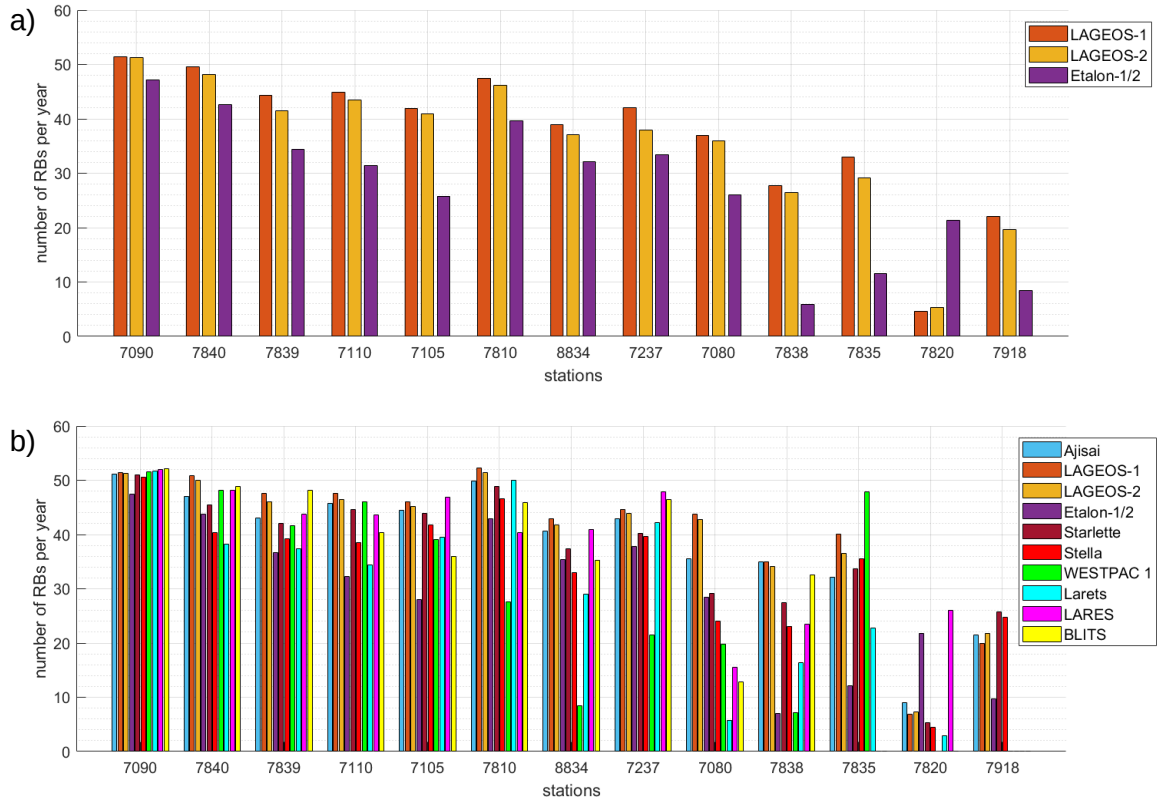

Figure 12: Number of RBs per year per satellites and per station: a) from the 4-satellite solution and b) from the 11-satellite solution The shown stations are: *CDP Pad ID 7090* – Yarragadee (DOMES no. 50107M001, Australia); *CDP Pad ID 7840* – Herstmonceux (DOMES no. 13212S001, UK); *CDP Pad ID 7839* – Graz (DOMES no. 11001S002, Austria); *CDP Pad ID 7110* – Monument Peak (DOMES no. 40497M001, USA); *CDP Pad ID* 7105 – Greenbelt (DOMES no. 40451M105, USA); *CDP Pad ID 7810* – Zimmerwald (DOMES no. 14001S007, Switzerland); *CDP Pad ID 8834* – Wettzell (DOMES no. 14201S018, Germany); *CDP Pad ID 7237* – Changchun (DOMES no. 21611S001, China) *CDP Pad ID 7080* – McDonald Observatory (DOMES no. 40442M006, USA); *CDP Pad ID 7838* – Simosato (DOMES no. 21726S001, Japan); *CDP Pad ID 7835* – Grasse (DOMES no. 10002S001, France); *CDP Pad ID 7820* – Kunming (DOMES no. 21609S002, China); *CDP Pad ID 7918* – Greebelt (DOMES no. 40451M120, USA)

In order to assess the data basis for the calculation of the mean RBs, the RBs per year of selected stations for all satellites used are illustrated in Figure 12. Figure 12 a) shows the RB per year from the 4-satellite solution and Figure 12 b) those from the 11-satellite solution. The values are presented for the ten stations with the highest RB numbers (1470-1001 RBs for LAGEOS-1 in 11-satellite solution) and three stations with lower RB numbers (see Table 5).

For the calculation of RBs in a 4-satellite solution, it can be seen that a similarly large number of RBs per year is available for LAGEOS-1 and LAGEOS-2 in each station. The combined solution of Etalon-1/2 has fewer RBs per year than the LAGEOS satellites. LAGEOS-1/2 are therefore observed more often per year by the individual stations or over a longer period of time (see Figure 12 a). Not all SLR stations track the Etalon satellites due to their high altitude (Sośnica et al., 2011) (see Figure 6).

When calculating the RBs in an 11-satellite solution (Figure 12 b), the number of RBs per year shows that the number of RBs per year for the satellites LAGEOS-1/2 and Etalon-1/2 increased

slightly. As an example, station Herstmonceux (DOMES no.13212S001, UK, Code 7840) shows an increase number of +1 RB/yr and station Greenbelt (DOMES no. 40451M105, USA, Code 7105) by +5 RB/yr, each for LAGEOS-1. Since in the 11-satellite solution more observations are available due to the higher number of satellites, the number of observations of the individual stations also increases and thus also the value of the RB per year. Figure 13 and Figure 14 exemplarily show the global distribution of stations that observed LAGEOS-1, together with the maximum number of RBs for each station for the 4- and 11-satellite solution. Individual stations are added in Europe and Central Asia in the 11-satellite solution. In total, the number of stations for LAGEOS-1 increases from 106 (4-satellite solution) to 112 (11-satellite solution). Furthermore, Figure 14 shows that the number of stations with more than 1000 RB has increased from 7 to 10 stations.

The seven added LEO satellites (see Table 1) have been observed with a similar frequency as the four satellites already in use whereas Starlette seems to have been observed less often by frequently performing stations than other satellites. WESTPAC 1 was only tracked by very frequently observing stations in its short duration. Some satellites like Larets, LARES or BLITS were not observed by individual stations (e.g., station Greenbelt (DOMES no. 40451M120, USA, Code 7918)). Therefore, stations that observe less frequently and do not provide as reliable results as the five best observing stations should rather be excluded in the RBs calculation.

No values are lost for the LAGEOS and Etalon satellites by the computation of the weekly RB solutions between the 4- and 11-satellite solution. Additionally, the seven LEO satellites were observed similarly well. Consequently, the 11-satellite solution can be used for the mean value calculation of RBs.

Table 5: Statistical data of LAGEOS-1 observing stations of the 11-satellite solution (i.a. top ten stations) (see also Figure 12)

CDP Pad ID	DOMES no.	city (country)	number of RBs	number of observations	observation period [yr]	RB/yr
7090	50107M001	Yarragadee (Australia)	1470	269572	28,5941136	51,41
7840	13212S001	Herstmonceux (United Kingdom)	1454	157544	28,5941136	50,85
7839	11001S002	Graz (Austria)	1361	110250	28,5749487	47,63
7110	40497M001	Monument Peak (USA)	1360	116333	28,5941136	47,56
7105	40451M105	Greenbelt (USA)	1316	101634	28,5941136	46,02

CDP Pad ID	DOMES no.	city (country)	number of RBs	number of observations	observation period [yr]	RB/yr
7810	14001S007	Zimmerwald (Switzerland)	1234	204863	23,5920602	52,31
8834	14201S018	Wettzell (Germany)	1225	86855	28,5749487	42,87
7237	21611S001	Changchun (China)	1137	72498	25,4510609	44,67
7080	40442M006	Mcdonald Observatory (USA)	1111	40599	25,3744011	43,78
7838	21726S001	Simosato (Japan)	1001	60952	28,5941136	35,01
7835	10002S001	Grasse (France)	500	26002	12,495551	40.01
7820	21609S002	Kunming (China)	94	2544	13,5687885	6.93
7918	40451M120	Greenbelt (USA)	52	1868	2,60643395	19.95

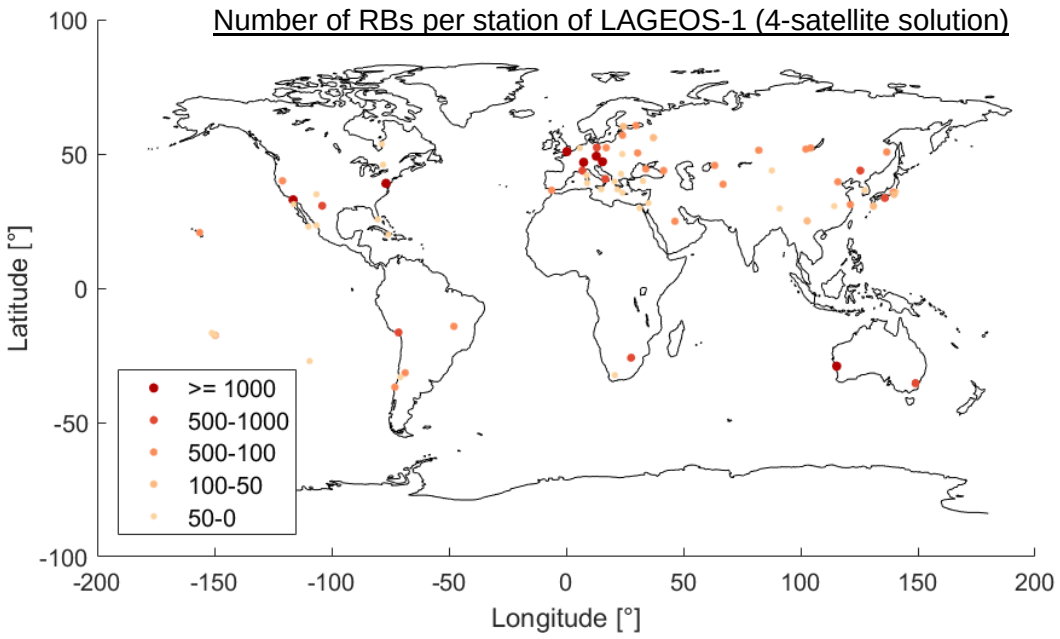

Figure 13: Global distribution of stations observing LAGEOS-1 of the 4-satellite solution. Shown in color are the number of RBs per station.

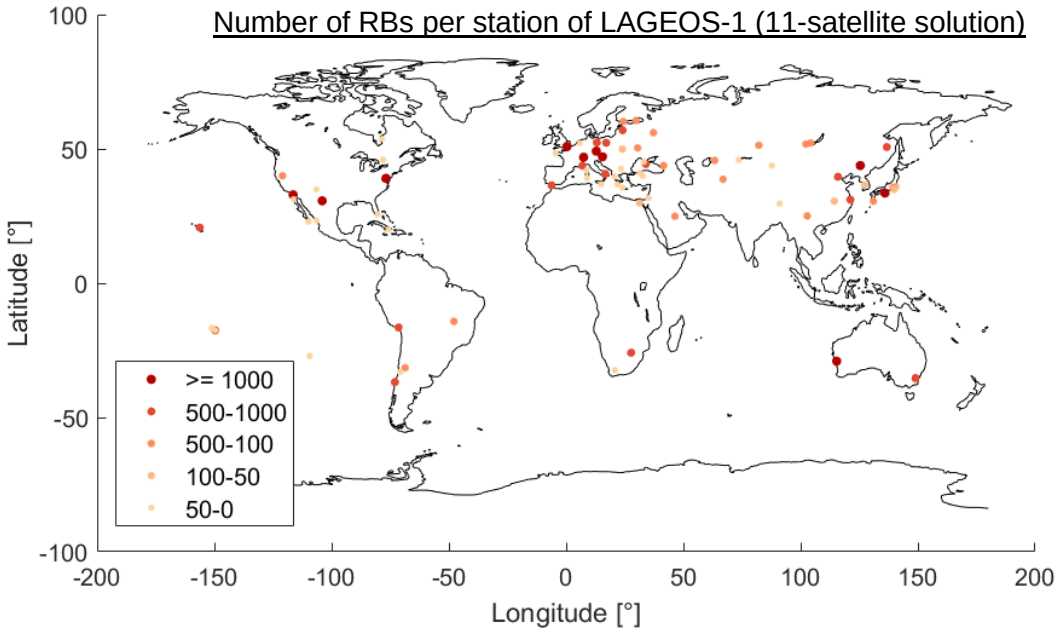

Figure 14: Global distribution of stations observing LAGEOS-1 of the 11-satellite solution. Shown in color are the number of RBs per station.

4.3 Weighted mean RBs and RBs of the DHF

Weighted standard deviation and weighted RMS value

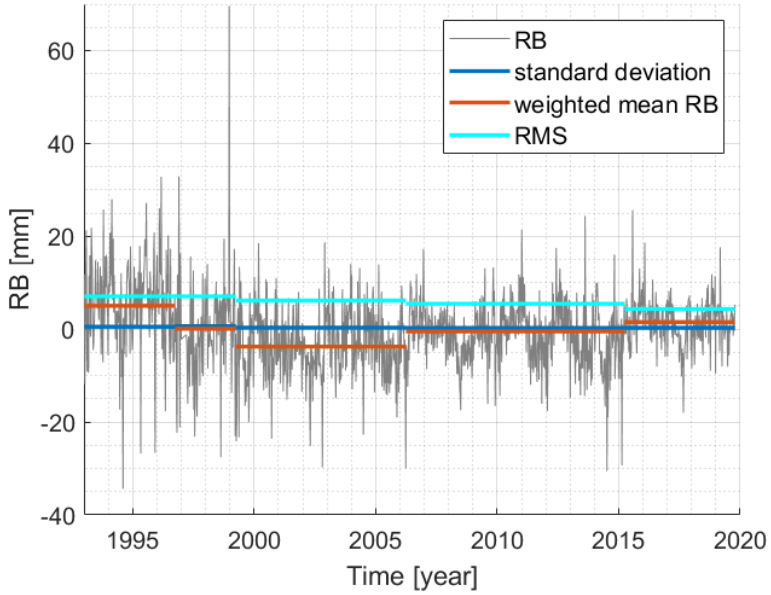

Figure 15: Calculated weighted mean RBs for the station Yarragadee observing LAGEOS-1 of the 4-satellite solution.

The calculated weighted mean RBs for the SLR Station Yarragadee (DOMES no. 50107M001, Australia, CDP Pad ID 7090) are illustrated in orange in Figure 15. As mentioned in chapter

3.2 and shown in Figure 15, the station Yarragadee (DOMES no. 50107M001, Australia, CDP Pad ID 7090) has a very long observation time series and small RBs. The time periods of the mean values are between 2.5 years (1996.75-1999.25) and nine years (2006.25-2015.25) long. The differences between the individual mean RBs are between 2 mm and 5 mm in absolute values. The smallest difference of two consecutive mean RBs of about 2 mm occurs in the year 2015.25 because the RB values for the last mean are slightly greater than the values for the mean between 2006 and 2015. The station history log shows that in 2015.14, a jump in the station time was noticed. A data impact of 3 was noted, which means the impact of the jump in the station time has a significant influence on the SLR measurements at this time[19]. The threshold for the steps to connect two mean values are chosen to be small at the beginning (see Figure 10) in order to detect such small differences in the time series of the RBs at excellent performing SLR stations.

The weighted standard deviation of the weighted mean RBs is posed in dark blue and the associated weighted RMS value is posed in light blue. The weighted standard deviation shows the dispersion of the RB values in the data of the respective time period, where some RB values are higher weighted than others. It indicates how well the mean values are determined. The weighted RMS values w.r.t. the weighted mean RBs show how strong the weekly RB values scatter around the calculated mean value. The standard deviation, as well as the RMS value, should be as small as possible. Because the greater the standard deviation and the RMS value, the stronger the dispersion and the worse fits the calculated mean to the RB values.

For the station Yarragadee (DOMES no. 50107M001, Australia, CDP Pad ID 7090) the weighted standard deviation has for all weighted mean RBs a value around zero between 0.28 mm (last time period) and 0.6 mm (second time period) (see Figure 15). The means fit the weighted RBs over the length of the period. By the majority, the longer the period, the smaller the weighted standard deviation. A short time period with a massive increase of RB values like in the second mean time period shows a large weighted standard deviation and a large weighted RMS value. The influence of the individual RBs per se is small for long periods, as long as the values do not deviate extremely from the range of variation within the periods. Considering their respective weights, the RBs do not deviate much from the weighted mean.

When evaluating the time periods of the time series of the RBs, it becomes obvious that the timing at which the time series shifts is not always uniquely identifiable. According to the algorithm presented in chapter 3, dividing the time series into time periods can only be done quarterly. Therefore, within such a quarterly section, there could be single values that are larger

[19] https://edc.dgfi.tum.de/en/stations/7090/station_history_log/, last access: 03-25-2022

or smaller than the other values in this section. These larger or smaller values are assigned by the quarterly division to a time period, from whose mean value they deviate more strongly than to the mean value of the preceding or following time period. These differences arise because most of the values in the quarterly section appear to be more heavily weighted and fit the assigned mean better. Therefore, the mean calculation should be more discriminating in selecting well-matched values. This approach could reduce both the standard deviations and the RMS value for the affected time periods.

Furthermore, when considering the outliers in the time series of the RBs, modifications of the technical measurement components (e.g., station clock) at the respective station should be taken into account. For this, reliable information on all stations for which mean values are to be formed is necessary. Thus, also outliers, which lay within the range limited by the outlier threshold and were not detected thereby, could be taken from the data set for the mean value computation. These unrecognized outliers are surrounded by even smaller RB values that vary around zero. However, an unrecognized outlier can only be removed from the data series if representing a random error. The data value must not be larger than the surrounding RBs due to, e.g., clock changes, system updates or earthquakes. If this is the case, the undetected outlier must be treated individually in the mean value calculation. In the case of the time series of the station Yarragadee (DOMES no. 50107M001, Australia, CDP Pad ID 7090) (see Figure 15), a random error would result in a lower RMS value or a different time period over which the mean value is calculated.

Comparison of the calculated RB to the given RB in the DHF

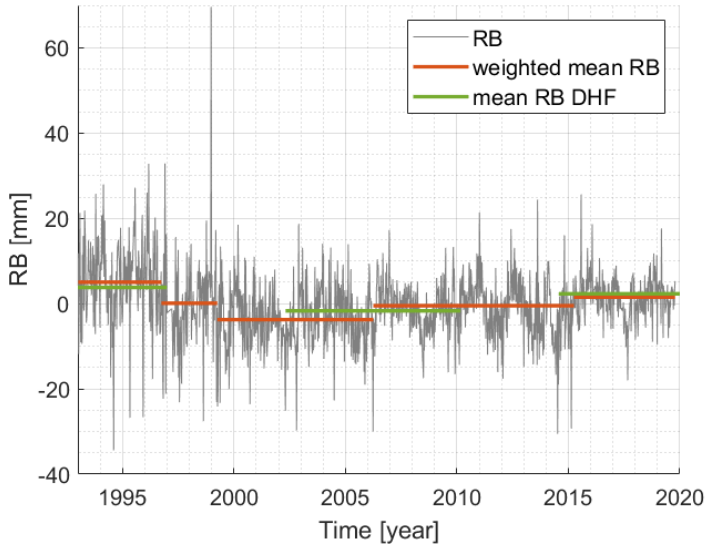

Figure 16: RB time series of the station Yarragadee observing LAGEOS-1 of the 4-satellite solution and the related mean RB value of the DHF

The section before shows that the weighted means fit well to the weekly RBs values. In this section, the calculated mean values are compared with the given mean values in the DHF from the ILRS CC. This is shown using the station Yarragadee (DOMES no. 50107M001, Australia, CDP Pad ID 7090) in Figure 16. In orange are the calculated weighted mean values and in green the mean RBs from the DHF. It can be seen that in the DHF not for each time period of the data series an RB is given. For the time periods 1997 to mid-2003 and 2010 to mid-2014, no explicit mean RB is specified. In these time periods, the mean RB used in the analysis of SLR observations is zero.

Since the data basis between the calculated RB and the RB of the DHF are different (see Table 4; DHF based on combined solution), the mean values cannot be compared directly with each other. However, the DHF with its values provide a framework in which the calculated mean value should be. Furthermore, in this thesis, the mean values were weighted (see chapter 3.2), while the exact calculation of the mean values in the DHF cannot be reproduced since no official publication on the computation algorithm is currently available. The first and last time periods overlap with the predefined RB time period in the DHF. The obtained values are also close to the pre-specified RB value of the DHF.

For the time period 2002 to 2010 of the DHF, two other time periods were specified for the station Yarragadee (DOMES no. 50107M001, Australia, CDP Pad ID 7090) in this thesis. According to the method described in chapter 3, the values that lie in the time period of the DHF fit partly to the values in the years before the time period and after the time period. The time periods can also differ due to the determination of the minimum length of a time period. In addition, as mentioned above, the different data sets are of importance, as well as the consideration of influences on the respective measurement at the time of measurement (e.g., clock errors, earthquakes). Despite the different time periods for the station Yarragadee (DOMES no. 50107M001, Australia, CDP Pad ID 7090), the mean values of the three time periods are close to each other.

The time periods of the mean RBs of additional stations included in the DHF were also comparably chosen to the predefined time periods. The mean RBs were in a similar range of values in each case. The results of the comparison of the weighted mean RBs with the mean RBs from the DHF using the example of the station Yarragadee (DOMES no. 50107M001, Australia, CDP Pad ID 7090) can thus also be applied to the other stations present in the DHF and calculated in this thesis.

Overall, it can be said that the weighted mean values of this thesis fit well to the mean RBs values of the DHF and thus the choice of the sections according to the method described in this work is valid and usable.

4.4 Analysis of the orbit parameters

The orbits with the derived mean RB values are calculated using DOGS-CS for a time span of more than 27 years (between 1993 and 2021). The parameters computed in this process allow an assessment of the accuracy of the orbits.

Comparison between orbit solutions of the DTRF2020 solution and the options

For the comparison of the calculated orbits with the orbits calculated using the DTRF2020 parameters (published in the ILRS DHF), the satellite LAGEOS-1 is used since it represents an important component in the ITRF calculations, and it is part of all computations.

Figure 17 shows the mean values for seven parameters of the respective calculations of the orbit of LAGEOS-1. The black polygon represents the respective reference value of each parameter. All values inside the polygon (grey shaded area) indicate lower values than the reference value. The values outside the reference polygon represent values greater than the reference value.

In Figure 17, the light blue curve shows the orbit parameters of the reprocessed data for the 4-satellite solution. The turquoise graph shows the orbit parameters of the reprocessed data for the 11-satellite solution (SSEM PP-like data). Both graphs (light blue and turquoise) form the orbit parameters for the weekly estimated RB values. The light blue graph for the 4-satellite solution represents the validation data. The orbit parameters for mean RBs values are described by the other five graphs. The dark blue graph represents the parameters of the DTRF2020 solution. This graph depicts the values that have been achieved so far using the RBs of the DHF. The parameters of the weighted averages are shown in the options (yellow, purple graph (option 1), red and green graph (option 2)).

The weekly solutions are closer to the reference polygon than the DTRF2020 solution (except empirical acceleration along-track (cosine)). The parameters of the weekly solution of the 11-satellite solution fit the reference polygon best overall (turquoise curve). Due to the weekly RBs used, influences can be compensated better than with long mean RB values. Thus, the reference values are more likely to be reached. The disadvantage of this is that geophysical effects (e.g., tides, loading effects, mass variations) are compensated, which should be preserved in the observation.

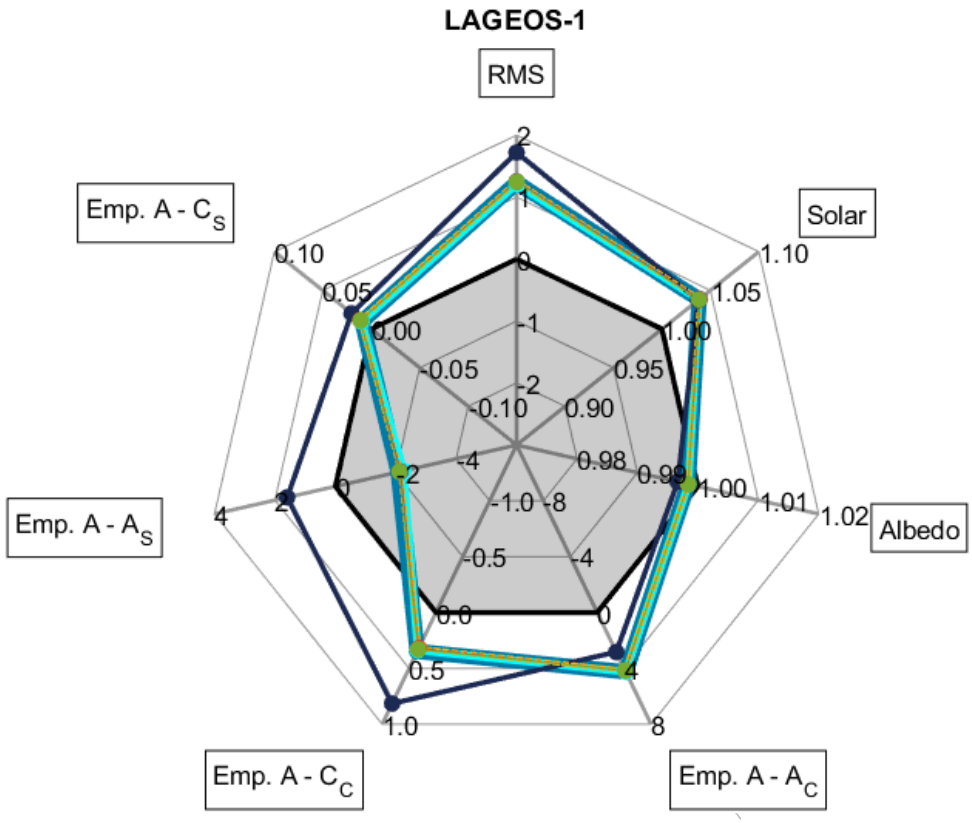

RMS	Root Mean Square of observation residuals [cm]	
Solar	Solar radiation pressure	scaling factors
Albedo	Earth Albedo	
Emp. A – A_C	Empirical Acceleration – Along-track (Cosine) [mm/d^2]	amplitudes
Emp. A – C_C	Empirical Acceleration – Cross-track (Cosine) [mm/d^2]	
Emp. A – A_S	Empirical Acceleration – Along-track (Sine) [mm/d^2]	
Emp. A – C_S	Empirical Acceleration – Cross-track (Sine) [mm/d^2]	

Figure 17: Orbit parameter of LAGEOS-1

The orbit parameters of the different processing options show very similar results to the weekly solutions and thus to each other. The similarity of the results is recognizable, since the graphs of the options overlap the turquoise graph. The smallest differences between the options are in the mean values of the empirical parameters at max. 10^{-5} m/d^2. In three of the four acceleration parameters, the parameters of the options lie closer to the reference polygon than

the parameters of the 11-satellite solution. Overall, this suggests that the estimated mean RBs fit the respective RB values of the time series well. In relation to the orbit parameters of the DHF solution for LAGEOS-1, the parameters of the options are closer to the reference polygon. The differences between the parameters of the available RB data sets are smaller for LAGEOS-2 and Etalon-1/2 than for LAGEOS-1. The RB values of the options are based on SLR data of DGFI-TUM, while the RB values of the DTRF2020 data set are taken from the DHF, which are based on the RBs of a combination of all ILRS ACs. Thus, one can state that the data basis only significantly influences the parameter results of LAGEOS-1. Considering the four satellites whose RB values are in the DHF, the parameters of the options fit well to the parameters of the DTRF2020. For LAGEOS-1, the orbit parameters of the options are closer to the reference polygon than the parameter of the DHF. This indicates that the functional model of the options better represents the observations. In this case, the mean values seem to be well determined and the increased number of stations leads to an improvement. Thus, with the mean RBs calculated according to the method from chapter 3, comparably good orbit parameters are achieved as by the RBs of the DHF.

A closer look at the individual options shows that option 2, with its more differentiated station selection, lies closer to the reference polygon. The option 2 with the 11-satellite solution (O2-11) does not achieve any concrete improvement w.r.t. option 2 with the 4-satellite solution (O2-4).

Looking at the individual parameters for LAGEOS-1, the largest differences between the respective parameter value of the options and the respective reference value are in the RMS value of the observation residuals. The deviations of the observation residuals should be minimal. The smallest differences to the reference value are in the parameters Earth Albedo scaling factor and the amplitudes of the empirical acceleration. The values are smaller than the respective reference value (except the DTRF2020 graph in the acceleration along-track(sine)).

Orbit parameter of the LEO satellite LARES

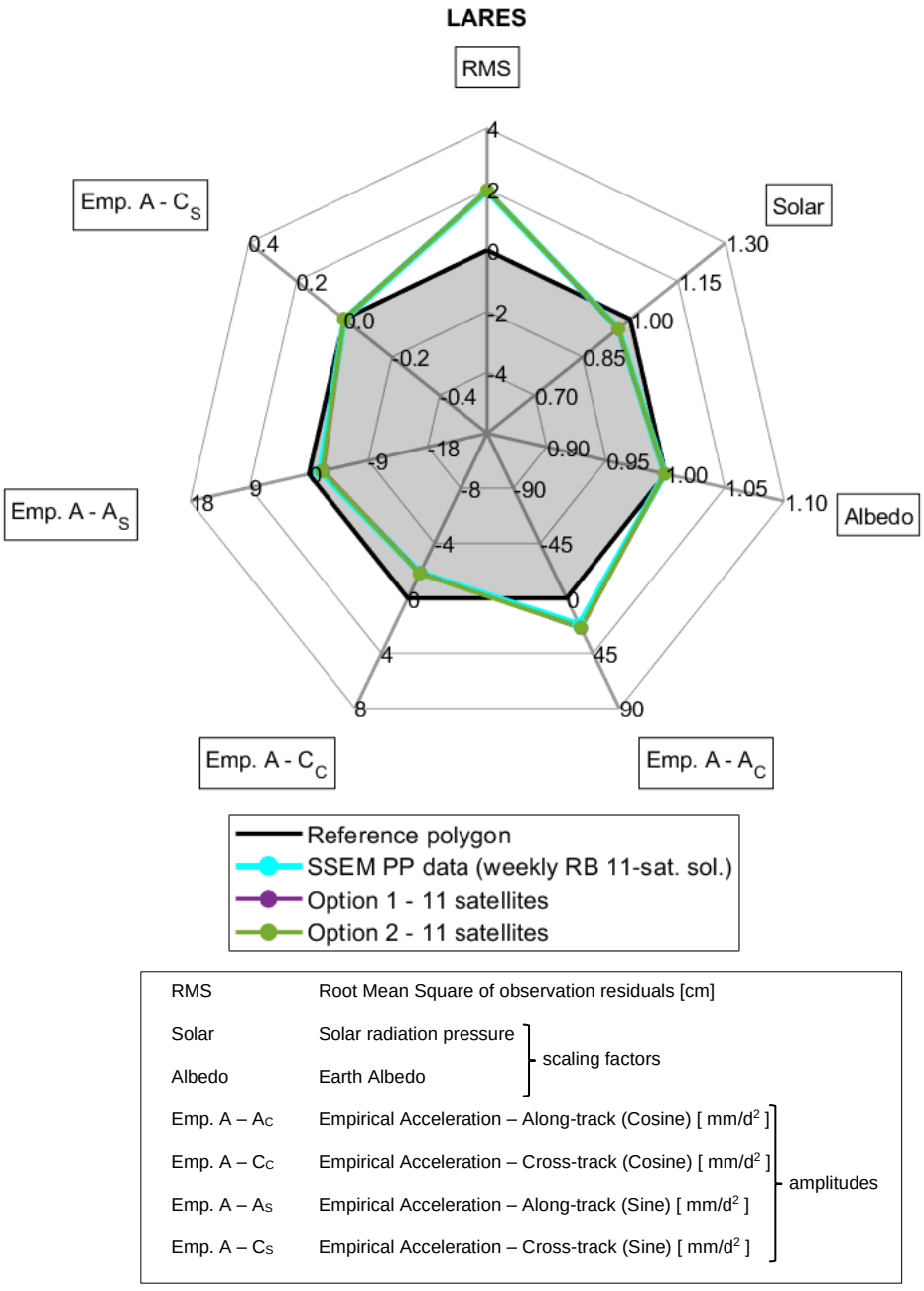

Figure 18: Orbit Parameter of LARES

In the following, the orbit parameters (Figure 18) of the LARES satellite will be discussed in more detail, representing the satellites whose mean RBs were determined for the first time in this thesis.

Regarding LARES, the used RB of all three available data sets lead to a good orbit representation. All parameters, except the RMS of the observation residuals, are close to the reference polygon and have small differences to each other resulting in overlapping graphs. In Figure 18, the parameters of the weekly RB values (11-sat-solution) best reflect the reference

values in 4 parameters (Earth Albedo; empirical acceleration along-track (cosine), along-track (sine), and cross-track (sine)). Concerning the two options of the 11-satellite solution, option 1 is closer to the reference value in the acceleration parameters. In contrast, for the RMS, solar radiation pressure and the Earth albedo parameters, option 2 leads to better results.

The results of the discussion of the orbit parameters for LARES are similar to results for LAGEOS-1 and can also be applied to the other satellites. All in all, it can be stated that the mean RB, according to the method from chapter 3 of the options, provide comparable results as the data of the DHF and the weekly RB.

Parameters of the individual orbit solutions of the options

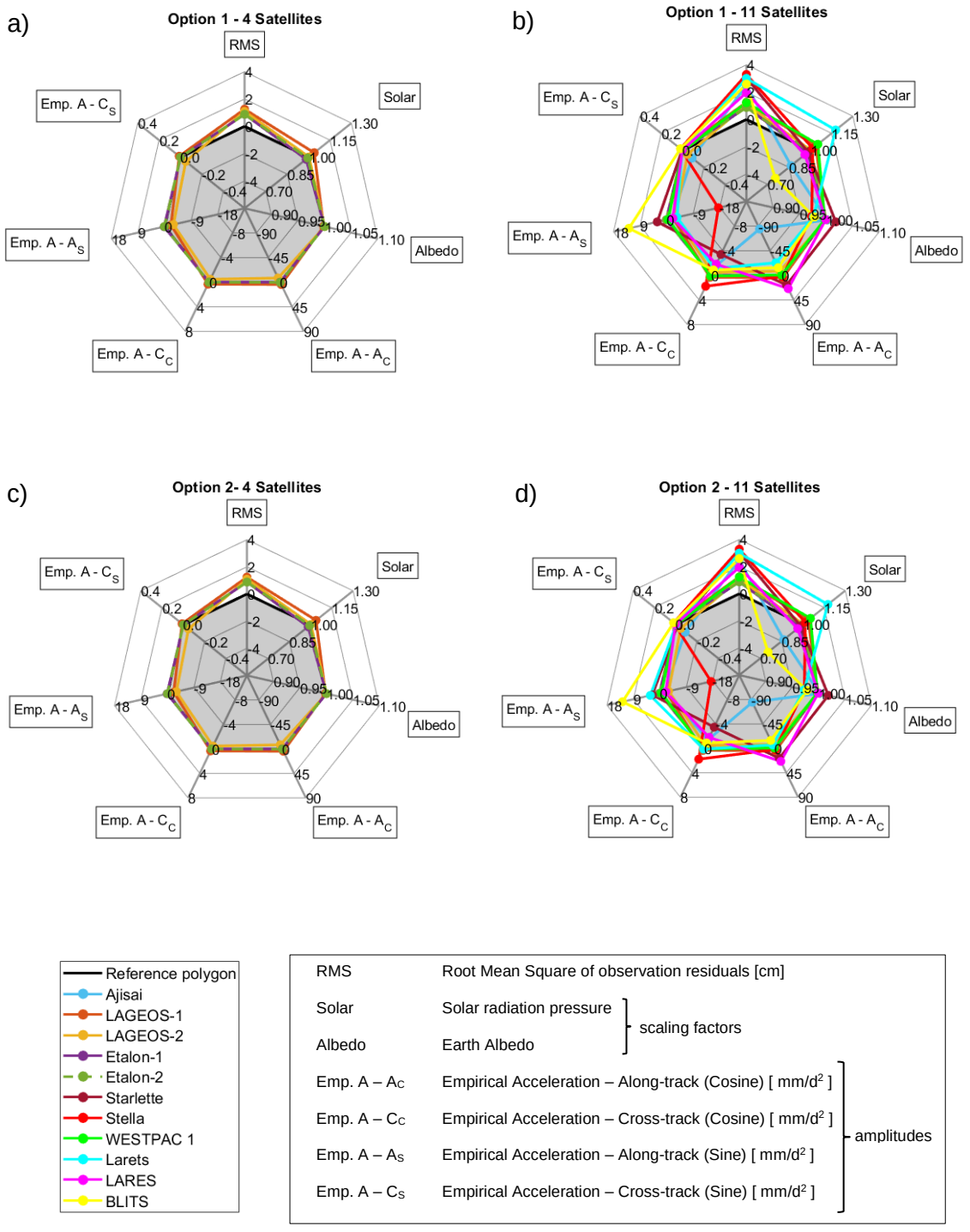

Figure 19: Orbit Parameters of the different options

As in Figure 17 and Figure 18, the reference values of the orbit parameters in Figure 19 are shown in black. In orange, yellow, purple and dark green the satellites LAGEOS-1/2 and Etalon-1/2 are depicted. All satellites show very similar values in the individual orbit parameters of the four calculated options and therefore match very well. In particular, the values of Etalon-1

and Etalon-2 are very similar. Since the satellites have a similar design and orbit (see Table 1), similarly sized orbit parameters are also expected when the same model and common RBs are used in the orbit computation. The values of all parameters are also close to the reference values. The largest difference from the reference value is the RMS value of the observation residuals. That may indicate, that the background models are not accurate enough. The Earth Albedo parameter values show the smallest differences w.r.t. the reference value. These are almost ideal at the value 1. Overall, the parameter values of the Etalon satellites are closer to the reference value than the LAGEOS satellite values.

Option 1 with 11 satellites Figure 19 b) shows a wide range of values within the individual parameters, except for the parameters Earth Albedo and the empirical acceleration cross-track (sine). For these parameters, the values for the individual satellites fit each other well with each other except a slight deviation of the satellites Starlette, Stella, Larets and BLITS. Furthermore, it can be seen that the RMS values of the residuals are only positive as the square sum of the residuals is calculated. Thus, the observations were estimated too large. When looking at the individual satellites, it can be seen that BLITS, Larets, Stella and Ajisai deviate strongly from the value range of the majority of the satellites in individual parameters (e.g., Solar Radiation Pressure). Especially BLITS is further away from the reference value of the single parameters compared to the other satellites. BLITS is the smallest and lightest satellite of the satellites used. Therefore, BLITS is more susceptible, e.g., for acceleration along-track (sine). Also, Stella, which has the lowest altitude with 804 km of all used satellites, is susceptible to accelerations along-track (sine). LEO satellites are strongly exposed to atmospheric drag due to their low altitude (Sośnica, 2015). This is also the reason why the parameter values in along-track differ more than the values in cross-track (±90 mm/d^2 vs. ±8 mm/d^2). The satellites whose parameter values deviate from the majority of the other satellite values are new in the calculation compared to option 1 with the 4-satellite solution (O1-4).

The satellite WESTPAC 1 shows very good parameter values compared to the other satellites with longer observation periods, despite the short observation period. Starlette shows a similarly long observation period and also a good RB per year ratio in the top stations compared to LAGEOS-1 but deviates more from the reference values of the individual parameters. This deviation may be due to more fluctuating observation values, causing the RBs to fluctuate more and be further away from zero on average than mean RBs for LAGEOS-1 observations. Another reason could be satellite-specific models, such as CoM satellite correction models. Furthermore, the area-to-mass ratio is higher than for LAGEOS-1/2, because Starlette is much lighter and smaller than the LAGEOS satellites. This higher

aera-to-mass ratio and the lower altitude make Starlette more susceptible to the attraction of the Earth's gravitational force (Gourine, 2012).

The second option O2 is shown in Figure 19 c) and d). When looking at the LAGEOS and Etalon satellites, for O2-4 the mean parameter values are similar to each other, to the reference values and thus to the results of O1-4 (Figure 19 a). Again compared to the other parameters, the albedo parameters are the best fit to each other and the reference value of one. The largest difference from the reference value is present in the RMS values of the observation residuals.

O2-11 shows a similar scatter within the parameters of the individual satellite solutions as option 1 with the 11-satellite solution (O1-11). The difference between the orbit parameters of the satellites for O1-11 and O2-11 is small (see Figure 19). Overall, the parameters in O2-11 are closer to the reference values than in O1-11. Especially for the satellite Larets the parameters of O2-11 improve compared to O1-11 (e.g., empirical acceleration along-track (cosine) and cross-track (cosine)).

The comparison between O2-4 and O2-11 shows that no obvious difference can be detected in the values for LAGEOS-1/2 and Etalon-1/2. The maximum difference for LAGEOS-2 in the RMS value of the residuals is -0.0046 cm, while the minimum difference in the empirical acceleration cross-track (sine) for Etalon-2 is $-5.52*10^{-8}$ m/d^2 .The differences between the parameter values of the options of one satellite are on average 10^{-6}. The orbit computation of these two options varies only in the number of satellites used. Since the difference in the parameter values between the two options is minimal for the four satellites, it has no effect, whether the weekly observations were determined in a 4-satellite solution or an 11-satellite solution, regarding the computation of the observations.

The results concerning the orbit parameters of the weekly RB solutions (reprocessed SSEM PP data) show that for O1-4 and O2-4, the graphs of the LAGEOS and Etalon satellites form a very similar shape w.r.t. the reference polygon. Thus, the parameters indicate good orbit quality. When comparing O1-11 and O2-11, the orbit quality is better for the O2-11 solution, because the individual parameter values scatter less around the respective reference value. When comparing the 4-satellite solutions to the 11-satellite solutions, the orbit quality is better for the 4-satellite options since the additional satellites in the 11-satellite options deviate more from the reference polygon. However, this is caused for the LEO satellites in the 11-sat solution due to their lower altitude and their higher area-to-mass ratio, as well as the tendency of shorter observation times

4.5 Analysis of the Helmert transformations parameter

Time Series of the Helmert transformations parameters

After the orbit calculation, Helmert transformations of the weekly solutions were performed w.r.t. the SLR-only TRF SLRF2014 (reference solution). The 7-Helmert transformation parameters are three translations, three rotations and the scale. These parameters were calculated for all options. In Figure 20, the time series of the translation parameters in x-, y- and z-direction, as well as the scale, are shown for all four options.
SLR is the only technique that realizes the origin and scale together with VLBI in the ITRF. In order to estimate the quality of the TRF datum parameters for which SLR is responsible in ITRF, these transformation parameters of a weekly solution to a multi-year solution are analysed.
The time series of the rotations are not shown in the following because the SLR solution is a loose constraint solution.

In the presented transformation parameters, the 11-satellite solution scatters more than the 4--satellite solution. The 4-satellite solutions vary between ±2 cm, while the 11-satellite solutions scatter up to ±5 cm in translation in the x-direction. The noise of the 11-satellite solutions decreases over time in the translation component in the z-direction and in scale. A trend toward zero over time is evident for all options. More stations, more observations or improved technology are available over time, making the result more stable and the noise decreasing.
The scale values of the options show a similar result to the translation components of the options. The values vary between ±1.5 cm (4-satellite solution) and ±2 cm (11-satellite solution). The 11-satellite solution is also noisier in scale.
For both the translation components and the scale, the curve of the parameters over time is similar in all options. Options 1 and 2 differ only by single outliers. The more precise station selection due to the number of RBs per year does not lead to a clear improvement in the transformation parameters. The additional stations in O1 are less suitable than the remaining stations in O1 or the stations in O2 for the Helmert transformation, because the Helmert transformation is high-sensitive w.r.t. the station selection. The Helmert transformation was performed iteratively. In the first iteration, all stations that exist in the respective week were used. Afterwards, the stations were removed according to a 3σ criterion in the iteration until reliable Helmert transformation parameters can be estimated.

That the 11-satellite solution scatters more than the 4-satellite solution despite more stations and more observations due to the larger number of satellites can have different reasons. On the one hand, mean RBs may not have been determined correctly in one or more satellites. On the other hand, the new satellites can bring uncertainties into the transformation. However, it is also essential to see that the reference solution ITRF2014 is a 4-satellite solution. This reference solution means that an 11-satellite solution was transformed to the 4-satellite solution. Thus, there are basically more significant fluctuations than with a transformation between the two 4-satellite solutions.

Frequency analysis of the Helmert transformations parameters

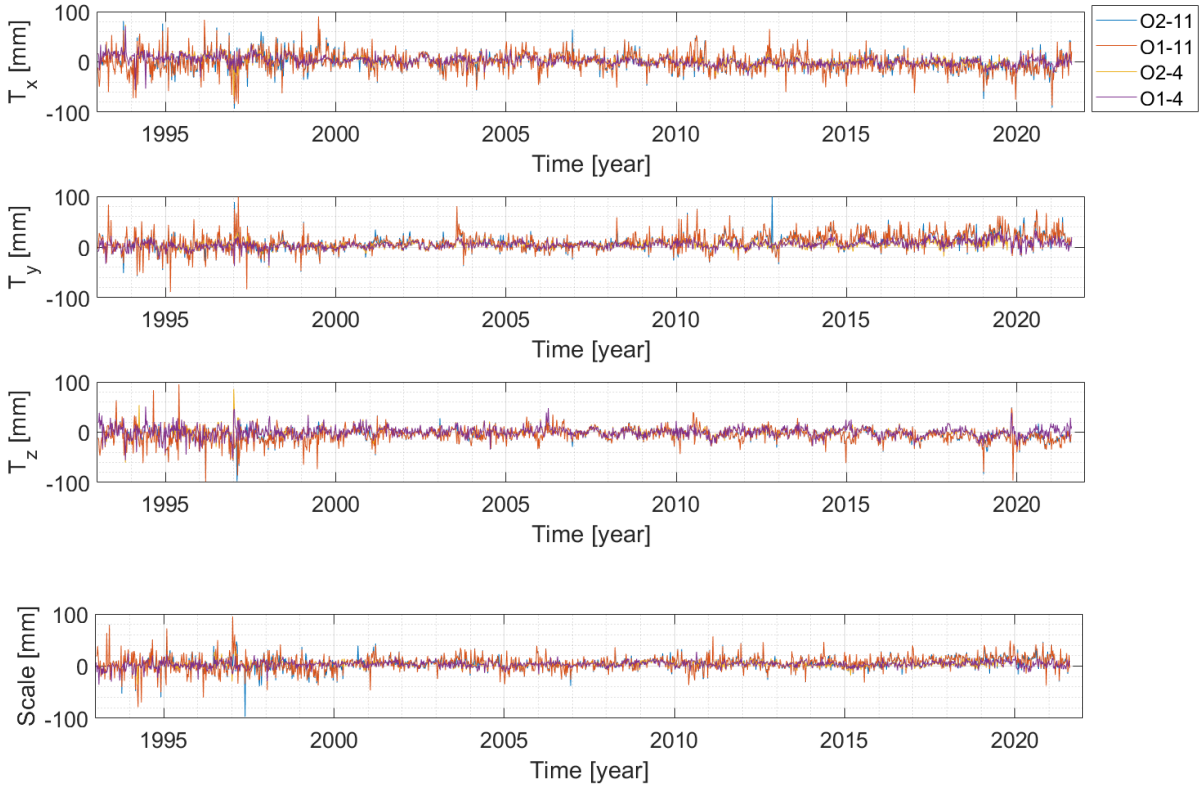

Figure 20: Time series of the Helmert transformation parameters translation and scale related to the four options O1-4, O1-11, O2-4 and O2-11.

In addition, a frequency analysis was performed for the translation components and the scale (see Figure 20). With the help of the frequency analysis, it is investigated to what extent systematics are present in the transformation parameters in addition to the annual signal. Figure 21 shows the spectra of the individual parameters for the four options. The time series of the translation components all show the main period at 365 days to 368 days. This period corresponds to the expected annual signal (period: 365.25 days). The amplitude in the annual signal is larger for the 11-satellite solution than for the 4-satellite solutions since the 11-satellite solution is also more scattered in the time series. There are only minimal differences between

the amplitudes of options 1 and 2 (< 0.2 mm), whereas the amplitude in the main period of option 2 is slightly higher (about 2 mm) (see Table 6).

In the scale, the amplitudes are clearly smaller than those of the translations. The maximum is nearly 3 cm for the 11-satellite solution. A yearly signal is recognizable for the 4-satellite solutions (365 days). The 11-satellite solutions, however, show a main period at 186 days. This period corresponds to a semi-annual signal (182.5 days).

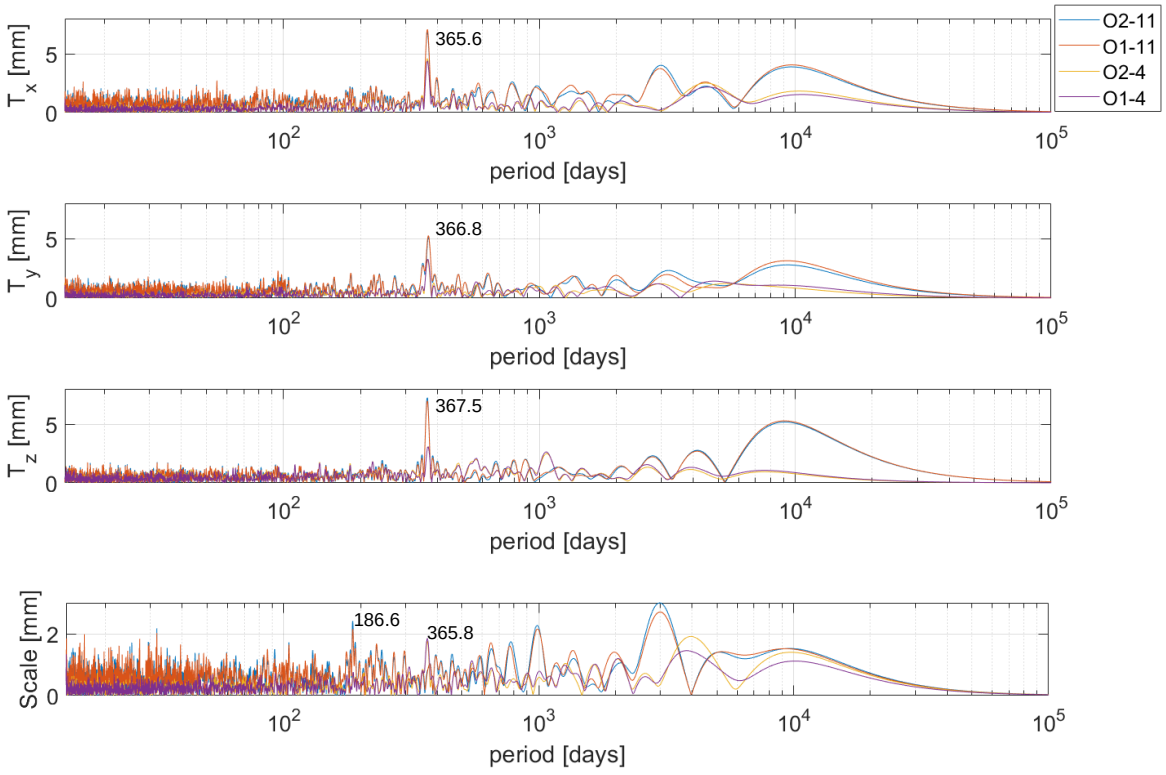

Figure 21: Amplitudes of the Helmert transformation parameters translation and scale for four options: option 1 - 4 satellites (O1-4), option 1 - 11 satellites (O1-11), option 2 - 4 satellites (O2-4), option 2 - 11 satellites (O2-11)

Figure 21 shows the mean amplitudes of the translation components for the individual options. For comparison, the amplitude range, according to Wu et al. (2017), is also shown. Wu et al. (2017) summarized different methods with which transformation parameters were calculated. The annual amplitude of the translations in the x-direction is larger than the values in Wu et al. (2017). In the amplitudes of the translations in the y-direction, the 4-satellite solutions are at the upper limit of the range of the values compared in Wu et al. (2017). The amplitudes of the 11-satellite solutions are also higher in this parameter. For the amplitudes of the translations in the z-direction, it can be seen from Table 6 that the 4-satellite solution is within the range of values of Wu et al. (2017) and the amplitudes of the 11-satellite solution are about twice the amplitudes of the 4-satellite solution. It can be seen that different data and methods lead to different amplitude values.

The weighted mean scale values for the 4-satellite solutions and the 11-satellite solutions of this thesis differ by about 2 mm (see Table 7). The 4-satellite solution with weighted mean RBs compared to the 4-satellite solution of Bloßfeld et al. (2018) shows a lower mean scale value. The differences between the mean values of the 11-satellite solutions and the 5-satellite solutions (exept 4-satellites + Ajisai) of Bloßfeld et al. (2018) are small. The mean scale values are between 4.3 mm and 5.6 mm. Due to a wrong CoM model for Ajisai, the mean value of the 5-satellite solution with Ajisai deviates from the mean values of the other 5-satellite solutions (Bloßfeld et al., 2018).

Table 6: Comparison of annual amplitudes of the translation components.

Data	**Amplitude T_X [mm]**	**Amplitude T_Y [mm]**	**Amplitude T_Z [mm]**
Wu et al. (2017)	1.3 – 2.9	2.6 – 3.2	2.9 – 4.2
Option 1 – 4 satellites	4.4	3.3	3.1
Option 1 – 11 satellites	6.9	5.2	7.0
Option 2 – 4 satellites	4.6	3.3	3.1
Option 2 – 11 satellites	6.6	4.9	7.2

Table 7: Comparison of weighted mean values of the transformation parameter scale.

	weighted mean value of scale [mm]	**Reference**
4-satellites (ref)	4.7	Bloßfeld et al. (2018)
10-satellites	2.9	Bloßfeld et al. (2018)
11-satellites	8.8	Bloßfeld et al. (2018)
4-satellites + Ajisai	16.0	Bloßfeld et al. (2018)
4-satellites + Starlette	5.0	Bloßfeld et al. (2018)
4-satellites + Stella	4.5	Bloßfeld et al. (2018)
4-satellites + Larets	5.2	Bloßfeld et al. (2018)
4-satellites + LARES	4.3	Bloßfeld et al. (2018)
Option 1 – 4 satellites	3.5	This thesis
Option 1 – 11 satellites	5.6	This thesis
Option 2 – 4 satellites	3.2	This thesis
Option 2 – 11 satellites	5.4	This thesis

5 Conclusion and Outlook

So far, only for LAGEOS-1/2 and Etalon-1/2, long-term mean RBs are available for defined time periods using the DHF from the ILRS ASC. This thesis determined long-term mean RBs for seven additional satellites observed using SLR. By determining the mean RBs for the LEO satellites Ajisai, Starlette, Stella, WESTPAC 1, Larets, LARES, and BLITS, reliable (bias-free) 11-satellite solutions could be calculated.

The 11-satellite solutions generally comprise more observations compared to the 4-satellite solutions. Due to the larger number of observed satellites, more stations are included in the RB determination, although the global distribution changes only minimally. The time series of observations of the individual stations are condensed because the 11-satellite solution increases the number of RBs per year of any station. This is especially the case for stations with fewer observations spread over the year than, for example, the high-performing stations Yarragadee (DOMES no. 50107M001, Australia, CDP Pad ID 7090) or Herstmonceux (DOMES no. 13212S001, UK, CDP Pad ID 7840). This results in the possibility to calculate mean RBs for more stations with similarly scattering RB values.

For calculating mean RBs, a method was developed in this thesis by which stepwise weighted mean RBs are calculated for each station according to a fixed scheme. This method ensures that, in addition to the station selection, the determination of the mean RBs for each satellite and each station proceeds in the same way and is thus comprehensible and comparable. The selection of stations for which RBs were calculated is based on the one hand on the number of observations (option 1: > 52 weekly RBs) and on the other hand additionally on the performance of the station (option 2: number of RBs per year). The stepwise extension of time periods allows perceiving even small changes between two time periods of 2 mm. This extension is especially relevant for very well observing stations, which at first sight have a uniform course of values of the weekly RBs. Thus, even small changes in the measurement system can be perceived at these stations, which influence the measurements, such as a clock change or error. In addition, the weighted calculation of the mean values makes it possible to reduce the influence of RBs with high standard deviations on the mean value. In comparison to known time periods and long-term mean RBs from the DHF, it can be seen that averaging using the method developed in this thesis and based on data from one AC (DGFI-TUM) leads to similar time periods as those of the combination of ACs (DHF).

The subsequent calculation of the orbits shows that the parameters of the options with the recalculated mean RBs have similar values compared to the orbit parameters of the DTRF2020 solution with the long-term mean RBs from the DHF. For LAGEOS-1, the recalculated mean

RBs can significantly improve the orbit parameters. For the LAGEOS and Etalon satellites, it can be seen that the choice of any processing option (O1 or O2) makes little difference in terms of the orbit parameters. However, in detail, the inclusion of the station performance shows a smaller difference between the parameter values and the reference values. In particular, for RMS values of the observation residuals, which are not minimal for all satellites, the values of option 2 are closer to the reference value. Thus, the computation of mean RBs for stations with dense, low scatter data series leads a functional model representing the observations more accurately.

In a further step, the translations and scale of the options were considered. The transformation of an 11-satellite solution to the SLRF2014, a 4-satellite solution, shows larger scatter in the time series. Regardless of the number of satellites and the number of used stations, all time series of the translational components show an annual signal. This signal is approximately 2-3 mm larger for the 11-satellite solution than for O1-4 and O2-4. In the time series of the scale, a semi-annual signal occurs for O1-11 and O2-11 instead of an annual signal. Due to smaller fluctuations and the only systematics due to the annual signal, the 4-satellite solution leads to a more stable result in amplitudes than the 11-satellite solution.

Returning to the research question of the beginning:

Can an 11-satellite solution be used for the ITRF?

The results of this thesis allow the conclusion that with the newly calculated RBs, an 11-satellite solution can be used for the ITRF. The orbits based on the recomputed RBs are qualitatively comparable to the orbits of the DTRF2020 solution, as well as to the 4-satellite solution for the LAGEOS and Etalon satellites. The transformation parameters are also in the same range of values as the parameters of the 4-satellite solution but scatter more. The mean scale values of the 11-satellite solutions are 2 mm larger than the mean scale values of the 4-satellite solution but show similar results to the 5-satellite solutions of Bloßfeld et al. (2018). Thus, the inclusion of additional spherical satellites in the ITRF leads to similar results.

For the RB calculation, certain assumptions were made in this work, such as the definition of outliers, the minimum length of a time interval, or the minimum difference between two mean values. All these criteria influence the chosen time periods and therefore the values of the mean RBs. Depending on the choice of the criteria, the result changes. Thus, the method for calculating mean RBs needs to be further investigated and improved. This choice requires accurate information on changes at the station (history logs) and a good CoM value for the respective satellite. Outsubo and Appleby (2003) and Otsubo et al. (2015) have determined CoM corrections for the satellites LAGEOS, Etalon, Ajisai, LARES, Starlette and Stella. The

determination of CoM correction can be enhanced through accurate measurement data (Outsubo and Appleby, 2003; Appleby et al, 2016). In this way, the functional models of the LEO satellites can be improved and thus the transformation parameters can be positively influenced.

Therefore, it is reasonable to extend the SSEM PP to more than four satellites to exploit the potential of LEO satellites. When selecting satellites, the quality of the individual orbits, as well as similar orbit parameter values of the individual satellites, should be considered. Regarding these aspects also 5 to 10 satellite solutions should be examined, whether these improve the origin and the scale concerning the 4-satellite solution and other satellite combination solutions.

Currently, the ILRS ASC is pursuing the goal of expanding the number of satellites from four to five and plans to include LARES for the next ITRF (Pavlis et al., 2018; Schillak, 2021).

List of Abbreviations

AC	Analysis Center
Ajisai	*Japanese for* Hydrangea
ASC	Analysis Standing Committee
ASI	Agenzia Spaziale Italiana / Italian Space Agency
BLITS	Ball Lens In The Space
CC	Combination Center
CoM	Center of Mass
DGFI-TUM	Deutsches Geodätisches Forschungsinstitut
DHF	Data Handling File
DOGS-CS	DGFI Orbit and Geodetic Parameter Estimation Software with the module Combination and Solution
DOMES	Directory of MERIT Sites
DORIS	Doppler Orbitography and Radio-positioning Integrated by Satellites
DTRF	ITRF solution of the DGFI-TUM
EOP	Earth Orientation Parameter
GNSS	Global Navigation Satellite System
IAG	International Association of Geodesy
ICRF	International Celestial Reference Frame
ID	Station Identification number
IERS	International Earth Rotation and Reference Systems Service
IGN	Institut National de l'Information Géographique et Forestière
ILRS	International Laser Ranging Service
ILRSA	official primary ILRS combination
ITRF	International Terrestrial Reference Frame

ITRS	International Terrestrial Reference System
JPL	Jet Propulsion Laboratory
LAGEOS	Laser GEOdynamics Satellite
LARES	Laser Relativity Satellite
LEC	Etalon combined solution
LEO	Low Earth Orbit
LLR	Lunar Laser Ranging
MEO	Medium Earth Orbit
O1-4	Option 1 and 4-satellite solution
O1-11	Option 1 and 11-satellite solution
O2-4	Option 2 and 4-satellite solution
O2-11	Option 2 and 11-satellite solution
RB	range bias
RMS	root mean square
SLR	Satellite Laser Ranging
SLRF	SLR TRF
SP3c	Spacecraft ID Correspondence Table for Orbit Exchange Files
SSEM PP	Systematic System Error Monitoring Pilot Project
Starlette	Satellite de Taille Adaptée avec Réflecteurs Laser pour les Etudes de la Terre
TRF	Terrestrial Reference Frame
UTC	Coordinated Universal Time
VLBI	Very Long Baseline Interferometry
WESTPAC	Western Pacific Satellite

List of Figures

List of Tables

Bibliography

Altamimi Z., Rebischung P., Métivier L., Collilieux X. (2016) ITRF2014: A new release of the International Terrestrial Reference Frame modeling nonlinear station motions. In: Journal of Geophysical Research: Solid Earth, DOI: 10.1002/2016JB013098

Appleby G., Wilkinson M., Luceri V., Gibbs P., Smith V. (2008) Attempts to separate apparent observational range bias from true geodetic signals. In: Proceedings of the 16th International Workshop on Laser Ranging, Poznan, Poland. URL: https://cddis.nasa.gov/lw16/docs/papers/net_1_Appleby_p.pdf

Appleby G., Rodríguez J. (2015) Proposed Pilot Study on determination of potential range bias in the ILRS stations. Proposal. URL: https://ilrs.gsfc.nasa.gov/docs/2016/Proposed_ILRS_AWG_Bias_PP_2015_16.pdf, available at: https://ilrs.gsfc.nasa.gov/science/awg/awgPilotProjects/awg_systematic_errors.html, last update 06-02-2016

Appleby G., Rodríguez J. (2016) ILRS Analysis Standing Committee pilot project on the determination of systematic errors in ILRS observations. First assessment of inter-AC consistency. URL: https://ilrs.gsfc.nasa.gov/docs/2016/asc_pp_bias.pdf, available at: https://ilrs.gsfc.nasa.gov/science/awg/awgPilotProjects/awg_systematic_errors.html, last update 06-02-2016

Appleby G., Rodríguez J., Altamimi Z. (2016) Assessment of the accuracy of global geodetic satellite laser ranging observations and estimated impact on ITRF scale: estimation of systematic errors in LAGEOS observations 1993-2014. In: Journal of Geodesy, 90(12), 1371-1388, DOI: 10.1007/s00190-016-0929-2

Bundesamt für Kartographie und Geodäsie (BKG; Federal Agency for Cartography and Geodesy) (2013) Satellite Laser Ranging (SLR). URL: https://www.iers.org/IERS/EN/Science/Techniques/slr.html, last access on 03-17-2022

Bloßfeld M. (2015) The key role of Satellite Laser Ranging towards the integrated estimation of geometry, rotation and gravitational field of the Earth. PhD dissertation, Deutsche Geodätische Kommission (DKG) Reihe C, No. 745, Verlag der Bayerischen Akademie der Wissenschaften, ISBN: 978-3-7696-5157-7

Bloßfeld M., Rudenko S., Kehm A., Panafidina N., Müller H., Angermann D., Hugentobler U., Seitz M. (2018) Consistent estimation of geodetic parameters from SLR satellite constellation measurements. In: Journal of Geodesy, 92, 1003-1021, DOI: 10.1007/s00190-018-1166-7

Bloßfeld M., Zeitlhöfler J., Rudenko S., Dettmering D. (2020) Observation-Based Attitude Realization for Accurate Jason Satellite Orbits and Its Impact on Geodetic and Altimetry Results. In: Remote Sensing 2020, 12(4), DOI: 10.3390/rs12040682

Doornbos E. (2012) Thermospheric Density and Wind Determination from Satellite Dynamics. Doctoral Thesis, Delft University of Technology. Berlin Heidelberg: Springer-Verlag. ISBN 978-3-642-25128-3, DOI 10.1007/978-3-642-25129-0

GGOS Global Geodetic Observing System (2022) Vision and Mission. URL: https://ggos.org/about/vision-mission/, last access on 03-17-2022

Gourine B. (2012) Use of Starlette and LAGEOS-1&-2 laser measurements for determination and analysis of stations coordinates and EOP time series - Utilisation des mesures laser de Starlette et LAGEOS-1&-2 pour la détermination et l'analyse des séries temporelles des coordonnées de stations et des EOP. In : Comptes Rendus Geoscience, 344(6-7),319-333, DOI : j.crte.2012.05.002

International Laser Ranging Service (ILRS) (2016) ILRS Terms of Reference (version November 17, 2016). URL: https://ilrs.gsfc.nasa.gov/about/termsofref.html, last update 06-20-2017, last access on 03-17-2022

Luceri V., Pirri M., Rodríguez J., Appleby G., Pavlis E.C., Müller H. (2019) Systematic errors in SLR data and their impact on the ILRS products. In: Journal of Geodesy, 93(11), 2357-2366, DOI: 10.1007/s00190-019-01319-w

Otsubo T., Appleby G.M. (2003) System-dependent center-of-mass correction for spherical geodetic satellites. In: Journal of Geophysical Research: Solid Earth, 108(B4), DOI: 10.1029/2002JB002209

Otsubo T., Kobayashi M., Takakura S. (2013) Subdaily Quality Check of Laser Ranging Data at Hitotsubashi University. Conference Paper. 18th International Workshop on Laser Ranging, URL: https://www.researchgate.net/publication/261288722_Subdaily_Quality_Check_of_Laser_Ranging_Data_at_Hitotsubashi_University, last access on 03-17-2022

Otsubo T., Sherwood R. A., Appleby G.M., Neubert R. (2015) Center-of-mass corrections for sub-cm-precision laser-ranging targets: Starlette, Stella and LARES. In: Journal of Geodesy, 89, 303–312, DOI 10.1007/s00190-014-0776-y

Otsubo T., Müller H., Pavlis E.C., Torrence M.H., Thaller D., Glotov V.D., Wang X. Sosnica K., Meyer U., Wilkinson M.J. (2018) Rapid response quality control service for the laser ranging tracking network. In: Journal of Geodesy, 93(11), 2335–2344, DOI:10.1007/s00190-018-1197-0

Pavlis E. C., Luceri C. (2018) Agenda for the Fall 2018 ILRS Analysis SC Meeting. Presentation. Presented at: 21st IWLR, 11-04-2018 in Mt. Stromlo, Canberra, Australia. URL: https://cddis.nasa.gov/lw21/docs/2018/splinter/ASC_CANBERRA_2018_PRESENTATIONS.pdf, last access on 03-17-2022

Pearlman M.R. (1984) Laser System Characterization. In: proceedings of the Fifth International Workshop on Laser Ranging Instrumentation Volume 1, Herstmonceux, U.K., p. 66-83

Petit G., Luzum B. (2010) IERS Conventions (2010). IERS Technical Note ; 36, Frankfurt am Main: Verlag des Bundesamts für Kartographie und Geodäsie, 2010. 179 pp., ISBN 3-89888-989-6

Plag H-P., Pearlman M. (2009) Global Geodetic Observing System Meeting the Requirements of a Global Society on a Changing Planet in 2020. Berlin Heidelberg New York: Springer-Verlag. ISBN: 978-3-642-02686-7, DOI: 10.1007/978-3-642-02687-4

Rothacher M. (2002) Combination of Space-Geodetic Techniques. In: International VLBI Service for Geodesy and Astrometry 2002 General Meeting Proceedings, p. 33-43, URL: https://ivscc.bkg.bund.de/publications/gm2002/rothacher.pdf

Schilak S., Lejba P., Michalek P. (2021) Analysis of the Quality of SLR Station Coordinates Determined from Laser Ranging to the LARES Satellite. In: Sensors 2021, 21(737), DOI: 10.3390/s21030737

Seeber G. (2003) Satellite Geodesy 2nd Edition. Berlin: Walter de Gruyter GmbH & Co. KG. ISBN: 3-11-017549-5, DOI: 10.1515/9783110200089

Seidelmann P.K. (Ed.) (1992) Explanatory Supplement to the Astronomical Almanac. Sausalito California: University Science Books. ISBN 0-935702-68-71-891389-45-9

Solomon, S. C. & the Solid Earth Science Working Group (2002). Living on a restless planet - Solid Earth Science Working Group Report 2002, NASA, Jet Propulsion Laboratory, Pasadena, California, URL: https://solidearth.jpl.nasa.gov/PDF/SESWG_final_combined.pdf, available at: http://solidearth.jpl.nasa.gov, last update 09-03-2021

Sośnica K., Jäggi A.,Thaller D. (2011) Availability of SLR Normal Points at ILRS Data Centers. Conference Paper. Conference: 17th International Workshop on Laser Ranging, Bad Kötzing, Germany

Sośnica K. (2015) Impact of the Atmospheric Drag on Starlette, Stella, Ajisai, and Lares Orbits. In: Artificial Satellites, 50 (1), DOI:10.1515/arsa-2015-0001

Strugarek D., Sosnica K., Arnold D., Jäggi A., Zajdel R., Bury G. (2021) Determination of SLR station coordinates based on LEO, LARES, LAGEOS, and Galileo satellites. In: Earth, Planets an Space, 73(87), DOI: 10.1186/s40623-021-01397-1

Wertz J.R. (Ed.) (1978) Spacecraft Attitude Determination and Control. In: Astrophysics and Space Science Library, v 73. Dorecht: Kluwer Academic Publishers. ISBN: 978-90-277-1204-2, DOI:10.1007/978-94-009-9907-7

Xu G. (Ed.) (2010) Sciences of Geodesy – I. Advances and Future Directions. Berlin Heidelberg New York: Springer-Verlag. ISBN: 978-3-642-11740-4, DOI: 10.1007/978-3-642-11741-1

Wu X., Kusche J., Landerer F. W. (2017) A new unified approach to determine geocentre motion using space geodetic and GRACE gravity data. In: Geophysical Journal International (2017), 209, 1398-1402, DOI: 10.1093/gji/ggx086